Andrés Ramírez Martínez

TALIN-1 IS A MECHANOSENSITIVE ADHESOME PROTEIN REGULATED BY ACTOMYOSIN CONTRACTIBILITY

TREBALL DE FI DE GRAU

Dirigit per la Dra. Anna Arola Arnal

Grau de Bioquímica i biologia molecular

UNIVERSITAT ROVIRA I VIRGILI

Tarragona

2014

Talin-1 is a mechanosensitive adhesome protein regulated by actomyosin contractibility

Results obtained from Yale Cardiovascular Research Center, under the supervision of Dr. Abhishek Kumar and Dr. Martin A. Schwartz.

Table of contents

Abstract

Mechanical forces exert important regulatory functions in processes such as differentiation, development and migration. Focal adhesions (FA) couple the extracellular matrix with the cytoskeleton and are main mediators in the interplay between physical changes and biochemical signals. Nonetheless, the regulation of tension in individual FA components has only been recently addressed. In this work, we report the use of a molecular tension biosensor in talin based on Förster resonance energy transfer (FRET). We found that tension on talin depended on the pulling forces transmitted by its direct association to actin. Disturbing actomyosin contractibility by small molecules or preventing direct actin binding increased FRET efficiency, indicating lower tension. These results provide direct information about the mechanism behind talin as a mechanical coupler between integrins and the cytoskeleton. We expect FRET tension biosensors to become a valid and useful tool for molecular tension measurements.

Introduction

Cells are able to respond to a plethora of stimuli. Physical forces are key players in differentiation[1], development[2], migration[3], vascular remodeling[4] and other relevant processes. There is a wide range of forces that can act upon cells (e.g. tensile, fluid shear stress, compression or expansion). In order to sense forces and to transduce them into biochemical signals (i.e. mechanotransduction) almost all organisms possess highly conserved structures specialized in responding to physical changes. As could be expected, most of these biomechanical sensors are located in the plasma membrane, where they participate in an intricate interplay between cell adhesion, extracellular matrix and the physical viscoelastic properties of the cell itself[5].

The most prominent mechanical sensors are focal adhesions (FA). FA are transmembrane multiprotein complexes of 2x3-10µm present in the basal membrane of adherent cells that couple the extracellular matrix (ECM) with the actin cytoskeleton[6]. The main component of FA are integrins but a total of 180 proteins have been reported so far to be part of FA, which are collectively known as the adhesome[7], including cytoskeletal, adaptor and signaling proteins. Among those, talin and other

proteins like filamin and α-actinin can provide a direct link to the actin cytoskeleton and consequently, may connect the response initiated in FA upon mechanical stress with downstream effectors.

Integrating the adhesome

Integrins

Integrins are transmembrane adhesion receptors (type I) associated in heterodimers of α and β subunits in a non-covalent form. There are 18 α and 8 β forms in vertebrates, which can associate into at least 24 heterodimeric receptor variations. Integrins are not present in the plasma membrane as monomers because they are transported to the surface after dimerization[8]. Integrin receptors resemble a big "head" and two "legs" (α and β) forming a bent capable of interacting with multiple ECM components. They consist of one N-terminal ectodomain, one transmembrane domain and a short cytoplasmatic tail in the C-terminus. Integrins can acquire a spectrum of different conformations but can be divided in three stages: (i) bent inactive, (ii) extended and (iii) fully activated extended integrin[9]. Regardless of the several nuclear magnetic resonance (NMR) studies of the cytoplasmatic region, there is no clear consensus about the structure of α or β subunits alone[10]. Nevertheless, β-integrins span two NPXY domains that are essential to recruit adaptor proteins. It is reasonable to attribute these structural discrepancies to the flexibility of the region, a domain that could be potentially stabilized by its association with other components of the adhesome.

Talin

In 1983, Burridge and Connell purified the protein known as talin from chicken gizzard smooth muscle[11]. Talin is a conserved protein of 2541 residues with an important role in integrin activation, actin cross-linking and coupling of focal adhesions with the cytoskeleton. There are two isoforms of talin that share 75% of identity: talin-1 (*Tln1*) and talin-2 (*Tln2*). While both show the same main function (i.e. link integrins to cytoskeleton) they present several differences: *Tln2* is not involved in Src (Proto-oncogene tyrosine-protein kinase Src) family kinase (SFK) activation and *Tln1* KD mice are not viable due to gastrulation defects whereas *Tln2* KD mice are viable and fertile[12]. Additionally, *Tln1* is required for platelet activation[13]. While *Tln1* 1 is ubiquitous, endothelial cells do not express *Tln2*. The two isoforms do not form heterodimers[14]. *Tln1* is the most studied isoform and, unless specified, it will be the one referred in this work as just talin.

From a structural point of view, talin is composed of three regions (**Fig.1**). A N-terminal FERM domain (F for 4.1 protein, E for ezrin, R for radixin and M for moesin) constitutes the talin head and

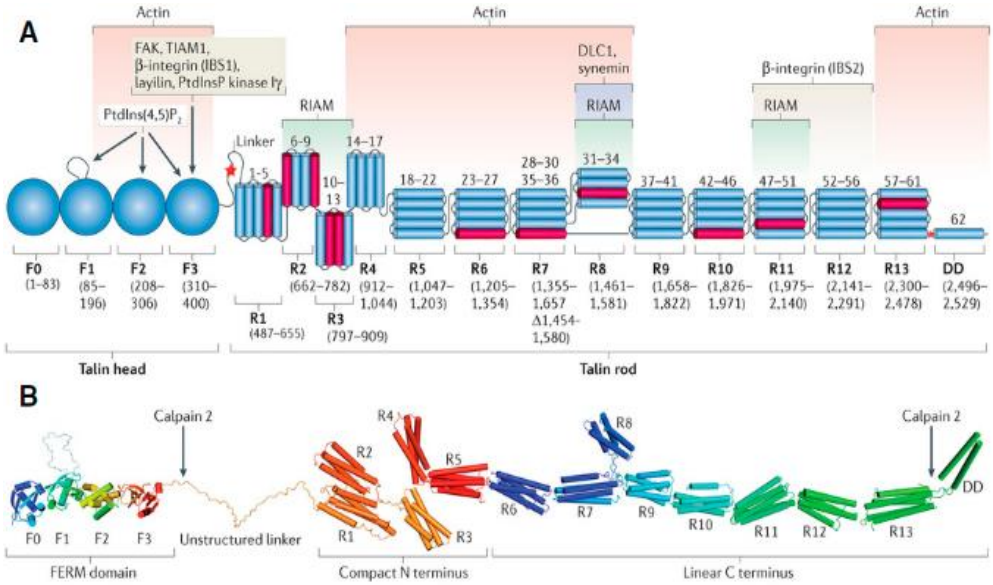

Figure 1. [A] Talin-1 domains and binding partners. Red stars indicate calpain-2 target sites. In pink, vinculin binding sites (VBS). B. Tridimensional structure of talin-1 [40]. TIAM1, T-cell lymphoma invasion and metastasis 1; DLC1, Deleted in Liver Cancer 1; RIAM, Rap1-GTP-interacting adaptor molecule; FAK, focal adhesion kinase;IBS2, Integrin-binding site 2; DD, homodimerization domain.

allows membrane translocation. This FERM domain is an unusual structure as F1 has a large insert (forming an unstructured loop) and there is an additional F0 domain besides F1, F2 and F3. F3 binds the hyaluronan receptor layilin[15] and the first NPXY motif of β-integrin tails through a phosphotyrosine-binding domain (PTB) made of seven β-strands, but F0-2 are also required for integrin activation[16]. The talin head is connected to the talin rod by a linker region with multiple phosphorylation sites[17] which can expand from up to 20nm if extended and is susceptible to calpain-2 proteolytic cleavage mediated by FAK (focal adhesion kinase)[18].The talin rod comprises 13 bundles of amphipatic α-helices (R1-13) and ends with a single C-terminal helix that acts as an antiparallel homodimerization domain (DD)[19]. However, the conformation of talin dimers remains unclear. The whole rod presents a large number of sequences able to bind other adhesome partners: 11 vinculin binding sites (VBS), 3 actin binding sites (ABS), one of them requires talin homodimerization to be active), and an additional integrin binding site (IBS2)[20]. A binding domain to α-synemin, an intermediate filament binding protein, has also been discovered[21] .

Talin is a main regulator of integrin activation and clustering. Using C-terminal fluorescent tagged integrins, a decrease in Förster resonance energy transfer (FRET) efficiency in K562 cells after the addition of a talin head has been observed[22]. Additionally, structural analyses suggest that the binding of talin to β-integrin may disrupt the association of both integrins destabilizing a salt bridge between them in their transmembrane domain (Arg995 in αIIb and Asp723 in β3)[23], with a concomitant increase in its affinity for ECM components and focal adhesion assembly[24]. These results seem to provide further evidence to the current model of integrin activation in which both legs need to dissociate to initiate downstream signaling. The PTB domain of F3 is necessary but not sufficient for inside-out β-integrin activation, as other proteins with the same domain are not able to induce integrin activation[25,26]. Consequently, there should exist additional interactions between both elements. A second integrin binding (IBS2) site is present in talin, yet it is located in the C-terminus. Evidence for IBS2 binding to β-integrin is contradictory: it has been detected by FRET[27] but superresolution fluorescence microscopy supports otherwise[28].

The rod is the element connecting β-integrin with the cytoskeleton. Calpain-2 increases talin binding to integrin *in vitro* and its knock-down leads to defects in focal adhesion disassembly in a FAK-dependent process[29]. Besides, calpain-2 removes the rod domain from the focal adhesion, resulting in loss of tension and higher focal adhesion turn-over. Both domains could also have potential additional regulatory roles in integrin recycling by themselves once cleaved[30]. Furthermore, talin KO mice fibroblasts adopt a rounded shape instead of their normal phenotype, an effect that can be rescued by full talin reexpression but not the talin head alone[31]. The C-terminal region mediates the association with actin through the last helix bundle (R13) and the C-terminal helix (DD). Actin cross-linking effects may be achieved by the presence of multiple ABS in the molecule[32].

There are several mechanisms for talin regulation. Talin can adopt two different conformations. In the globular configuration, the F3 region binds the R9 domain of the rod, impairing β-integrin association and leading to an autoinhibited state[33]. Talin can also stretch from 50nm in its globular conformation to 400nm in a vinculin dependent fashion after actomysin contraction[34]. Additionally, F3 can bind to FAK[35] and the C-terminal region of PIPK1γ90 (phosphatidylinositol-4-phosphate 5-kinase type 1 γ 90)[36]. In fact, talin remains inactive in the cytosol, and it translocates to the plasma membrane after PIPK1γ90 binding to the F3 subdomain (which is available independently of talin conformation). In addition, the talin head membrane-proximal surface contains basic residues with high affinity for acidic phospholipids that anchor it to the plasma membrane, and phosphatidylinositol 4,5-bisphosphate (PIP_2) can bind F3 and increase integrin binding. PIPK1γ90 can be phosphorylated by several kinases modulating its activity positively or negatively. These observations suggest a model where PIPK1γ90 would translocate talin to the membrane, which would then be activated by an increase in PIP_2 levels[20] (**Fig.2A**). Surprisingly, PIPK1γ90 affinity to talin is higher than β-integrin, a fact that raises the question about what additional mechanisms may be involved in talin activation and engagement in focal adhesions. In the autoinhibited state, the IBS2 may be hidden, as the talin head interacts with a rod region overlapping IBS2. Other F3 binding partners could also mask the binding of

IBS2 to β-integrin. These multiplicity of interactions might explain the differences in FRET and superresolution studies previously commented.

The talin-binding domain of vinculin can also promote talin membrane translocation and focal adhesion strengthening[37]. Talin possesses several VBS that bind vinculin with high affinity (K_d =15–40 nM) but purified molecules show a lower affinity (K_d =0.15-9μM)[38]. That discrepancy may be explained by the effect of mechanical forces on talin, which could expose VBS hidden inside the bundles. At the same time, vinculin competes with RIAM (Rap1-GTP-interacting adaptor molecule) (**Fig.2B**). Interestingly, RIAM and vinculin are mutually exclusive[39] and while RIAM is present in nascent adhesions, vinculin can be found in mature ones[40]. A possible explanation for such difference could be the mechanosensitive nature of talin: increasing tension may expose different binding domains (forces of 12pN applied by magnetic tweezers can expose cryptic VBS that would allow vinculin association[41]) and lead to an eventual transition from RIAM-talin nascent adhesions to mature vinculin-talin stable focal adhesions by vinculin cross-linking of actin and talin, hinting a physical tuning of talin affinity for vinculin during focal adhesion maturation. Actually, each component of the FA adhesions is under different tension: atomic force microscopy studies have demonstrated that it is necessary a tension around 30pN applied to α5β1 to reach maximum integrin stability[42] while each actin-myosin can exert a force of 6pN[43]. Talin is the main link between integrins and actin, forming part of the fibronectin–α5b1–(talin)–actin–myosin II complex. Thus, the control of the tension forces over this molecule are essential to control FA dynamics.

Competition among PTB-domain proteins can also result in talin inhibition. α-actinin, an adaptor protein that binds integrin and actin, exerts differential effects depending on the integrin observed, increasing talin binding to β1 integrins and decreasing it to β3 integrins[44]. Filamin is the best characterized example of competitive inhibition. There is an overlap of four residues between the β-integrin tail binding sites of filamin and talin[45]. Consistently, expression of migfilin, an adaptor protein whose binding site competes with integrin for filamin, increases integrin activation[46] but the *in vivo* function of migfilin is still unknown[47]. Integrin downstream signaling can also modulate the affinity of each protein toward the NPXY motif. For instance, the NPXY motif can be phosphorylated by SFK, inhibiting talin binding and integrin activation as a result. The kindlin family are proteins that may be involved in talin activation. Kindlins do not seem to bind to talin but are considered integrin coactivators that interact directly to integrin, even if their effects can vary depending on the integrin dimer and the kindlin isoform[48,49]. Through nanodisks (discoidal lipid bilayers of 8-16nm in diameter, wrapped by amphipatic domains[50])

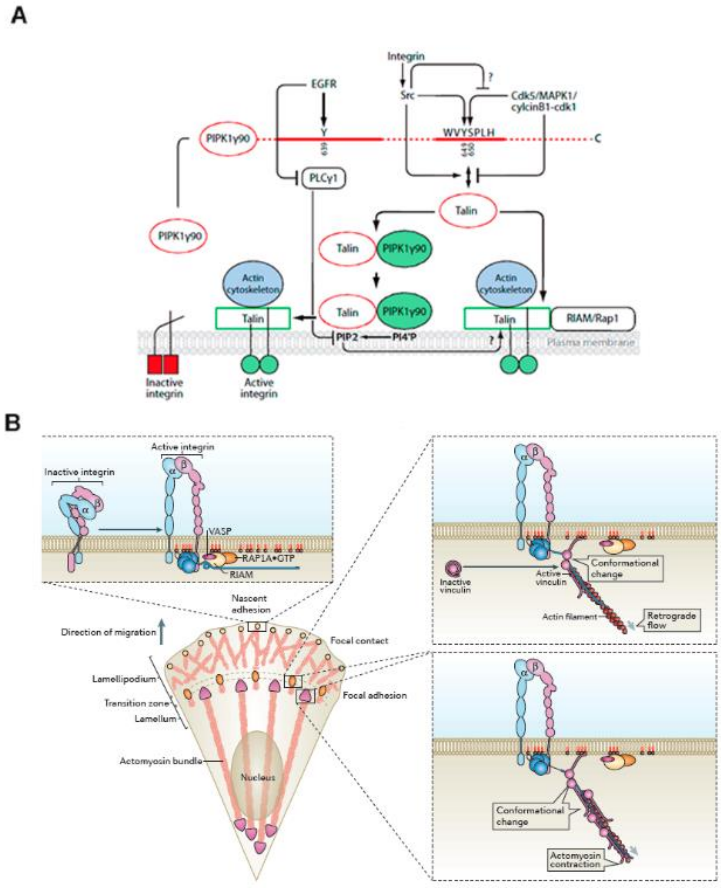

Figure 2. Signaling pathways that regulate talin activation. [A] Model for talin recruitment by phosphatidylinositol-4-phosphate 5-kinase type 1 γ 90 (PIPK1γ90)[20]. [B] Talin affinity for its binding partners changes during FA maturation[40]. Rap1, Ras-proximate-1; RIAM, Rap1-GTP-interacting adaptor molecule; EGFR, epidermal growth factor receptor; PLCγ1, Phospholipase C, gamma 1; Src, Proto-oncogene tyrosine-protein kinase Src; Cdk5, Cyclin-dependent kinase; MAPK, Mitogen-activated protein kinase.

and a clever use of mutations, it has been observed that kindlin effects are dependent on talin-mediated activation[51]. In general, all these interactions allow us to understand the intricacy of talin regulation as a consequence of an environment as complex as the adhesome.

Vinculin

Vinculin is an actin-bundling protein present in FA with functions in cell-matrix adhesion and cell-cell junctions[52]. It binds to several adhesome proteins, talin among them, and increases FA stability. In fact, vinculin depleted cells present less, smaller and more dynamic focal adhesions[53].

Vinculin does not bind directly to integrins, but it acts as a mechanical coupler by interacting with several other proteins. The affinity between vinculin head and tail is very high ($K_d < 10^{-9}M$)[54] and no ligand known to date shows comparable affinity values. Two models for its activation have been proposed: a combinatorial activation (two or more binding partners required for activation) and a simple activation by talin or α-actinin[55]. The conformational changes in vinculin activation have been observed *in vivo* using FRET microscopy: inserting yellow fluorescent protein (YFP) and cyan fluorescent protein (CFP) sequences in N and C- terminus respectively, a FRET efficiency decrease could be observed after vinculin activation by IpaA (invasion protein from *Shigella*)[56]. Using this FRET strategy, it was confirmed that talin alone was not enough to induce vinculin conformational changes but, instead, it required actin too[57].

In its active conformation, the tail dimerizes and vinculin acts as an actin cross-linker[58]. Surprisingly, FA present a small fraction of inactive vinculin, suggesting different pathways for recruitment and activation during assembly and disassembly[56]. Furthermore, vinculin can also modulate FAK and paxilin signaling inhibiting their phosphorylation[58,59]. Phosphoinositides may also regulate vinculin recruitment, as they compete with F-actin for vinculin binding, increasing FA turnover[60].

From a mechanical point of view, vinculin mediates force transmission: vinculin depleted cells exert lower forces on the ECM[61]. Combining FRET and an elastic domain composed of nanosprings, an innovative study developed a vinculin tension sensor that made possible to visually observe the forces experienced by vinculin[62]: in stable FA, tension across vinculin was around 2.5pN. Higher forces were observed during FA assembly and enlargement, whereas tension decreased with disassembly. However, vinculin recruitment and activation where force independent, as no significant changes happened in either case after actomyosin inhibition by Y-27632 mediated Rho-associated protein kinase (ROCK) inhibition and myosin IIa depletion by RNA interference. Even if talin stretching and exposure of additional VBS may be dependent on actomyosin contraction (and therefore, talin interaction with vinculin may have been inhibited by the treatments) the rest of binding partners could still retain vinculin in FA.

Actomyosin

Focal adhesions require a linkage to the actin cytoskeleton to form and mature. There are several adhesome components that mediate such connection: talin binds directly to β-integrin and actin, as do α-actinin (both of them associate with vinculin as well) and filamin[8]. Integrin β4 can associate with intermediate filaments, but that interaction has not been studied mechanically. In addition, myosin, an ATP-dependent molecular motor, is required to exert intracellular forces on the cytoskeleton, which may be transmitted to the ECM and allow an internal tension proportional to adhesion strength and, in that way, keep tensional homeostasis.

The term actomyosin refers to the complex of actin and myosin, which, in conjunction, mediate muscle contraction and other processes like migration, cell contraction and FA renewal. Actin is one of the most conserved proteins among eukaryotes, probably due to its high number of interacting partners. Actin may be able to tune its conformation is response to forces exerted by myosin II, but most studies so far have focused only on its role as force transmitter and its elastic deformation[63].

On the other hand, myosin are molecular motors that move through actin filaments in an ATP-dependent process. The myosin family is divided in around 20 classes that comprise 139 members[64], but they are similar in terms of structure. The current model for myosin contraction (**Fig.3A**) is called

the swinging lever-arm model[65]. In broad terms, an actin-bound myosin (actomyosin complex) binds an ATP molecule, inducing a conformational change in the motor domain that leads to actin disassociation. ATP is then hydrolyzed into ADP and inorganic phosphate (Pi). While binding ADP and Pi (pre-power stroke state), this complex binds actin again and releases Pi, an event that initiates the actual power stroke of myosin (i.e. its movement along actin). The ADP molecule is then released and the actomyosin complex is formed again, ready for another cycle. The conformational changes in the motor domain are small, but they are further amplified 10-fold in its distal domain by a level-arm domain. In fact, a 180º rotation of the level arm domain can reverse the direction of myosin movement[66].

Myosin II is the main generator of the necessary forces for locomotion, cell adhesion (dis)assembly and cytoskeletal tension. In addition, it also cross-links actin in a force-independent fashion[67]. The tension exerted by myosin II is under tight control both physically and biochemically. Forces lower than 2pN decrease 75-fold the detachment of myosin I from actin[68] and myosin II interacts with actin with a catch bond mechanism with an optimal force of 6pN, which is also the maximum force exerted by that molecular motor[69]. Myosin II is recruited to regions mechanically stimulated and external forces can restrain the lever arm, stopping the swinging cycle[70].

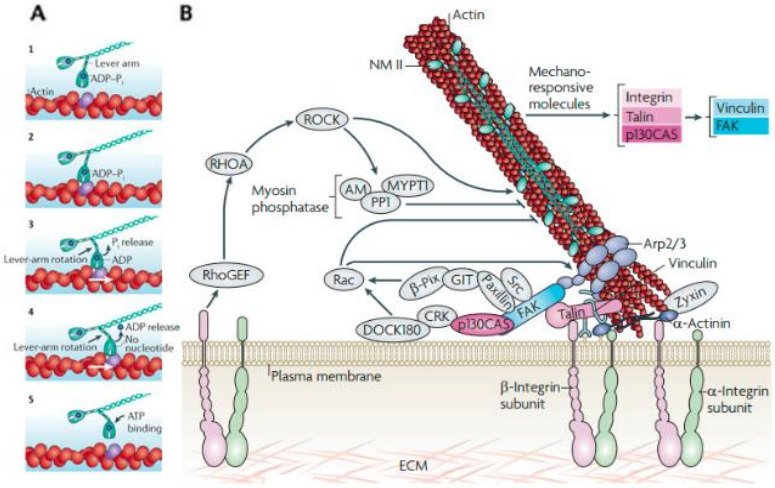

Figure 3. [A] The swinging lever-arm model for myosin contraction[139]. [B] Actomyosin regulation by focal adhesions[67]. Relevant acronyms are commented in text.

Phosphorylation of its two regulatory light chains (RLC) can activate myosin II. Myosin light chain kinase (MLCK) was the first kinase identified in myosin II activation[71]: it phosphorylates RLC, binds myosin and actin and may be stretched between myosin and actin during rearward flow, which could alter its autoinhibited state and activate myosin II. The ROCK family also phosphorylates MLC *in vitro*, as well as myosin phosphatase (MLCP).

Simultaneously, those kinases are regulated by members of the Rho GTPase family[72] (**Fig.3B**). Members of the Rho GTPase family modulate each other by nucleotide exchange factors (GEFs) and GTPase-activating proteins (GAPs). RhoA increases actomyosin contraction, the opposite effect of Rac1. However, Rac1, inhibits RhoGEF NET1 and activates p190RhoGAP, inactivating RhoA[73]. Myosin II kinetics and force bearing properties also change depending on which isoform expressed (NMII-A, II-B, or II-C.).

<u>Adhesome proteins act in concert to regulate focal adhesions</u>

Signaling in FA is a bidirectional process. Intracellular components can activate integrins and modulate their affinity to components of the ECM (inside-out activation). Besides, the extracellular ligands of integrins can trigger changes in the structure of the αβ heterodimer (outside-in activation) and provide information about the surroundings to alter the cellular adhesive capacity. In both pathways, mechanical stimuli can participate in integrin activation, either externally (matrix stretching, shear stress) or internally (actin polymerization, actomyosin contractibility). Integrin activation is an essential process that needs to be strictly regulated. For instance, integrin αIIb activation in platelet cells is a key step in thrombogenesis[74], and leukocytes can be retained at a site of infection after an increase in β2-integrin binding affinity to (intercellular adhesion molecule 1)/V-CAM (vascular cell adhesion molecule 1) receptors [75].

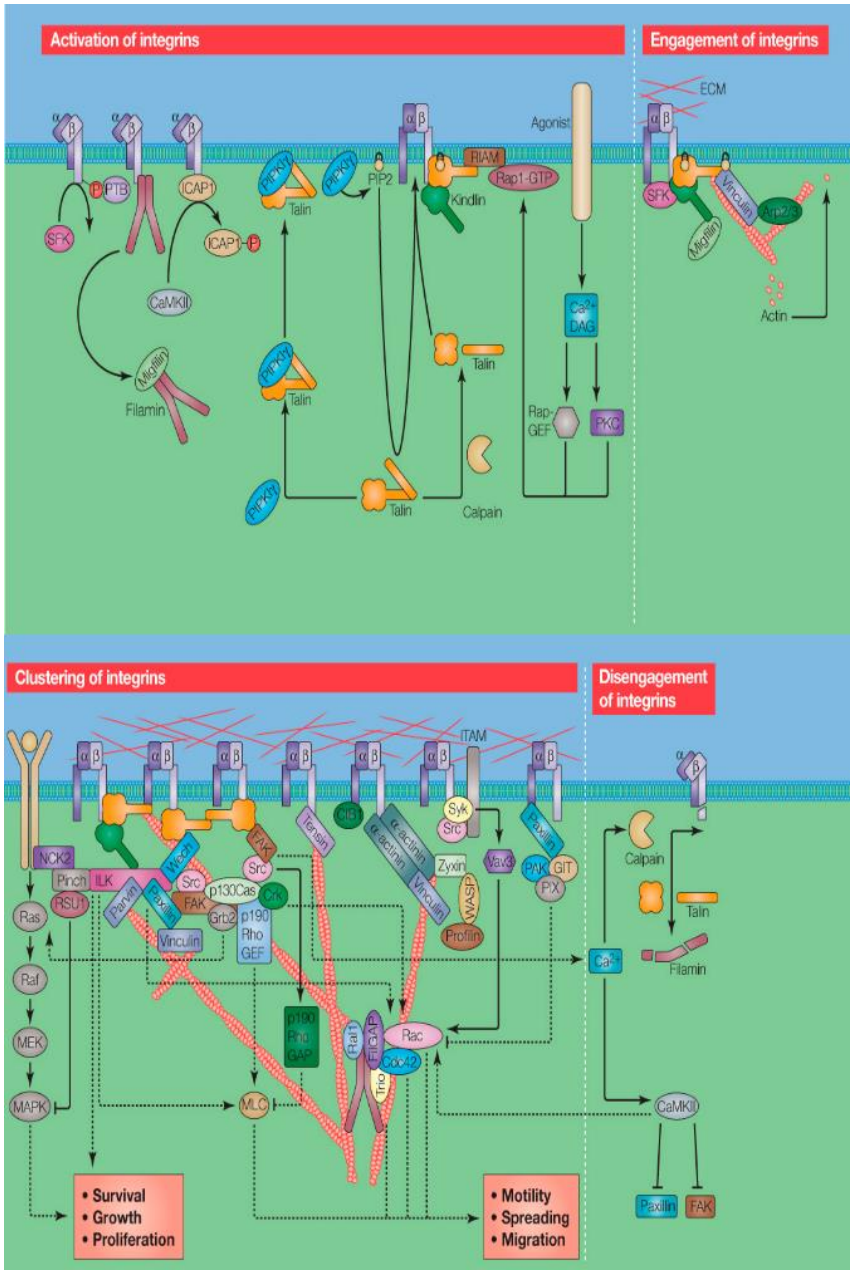

Figure 4. Main components of the adhesome and their role in focal adhesion dynamics[140]. Relevant acronyms are commented in text.

The activation process requires the dissociation of the integrin heterodimer (**Fig.4**). A critical factor in the heterodimer conformation is the tilt of each subunit relative to the plasma membrane[76]. α-integrin is perpendicular to the lipid bilayer, whereas β-integrin has an angle of 25º [16]. β-integrin binding to an extensive region of the talin FERM domain induces a decrease of 20º in β-integrin tilt, with a concomitant decrease of affinity between α and β-integrin transmembrane domains that leads, eventually, to their dissociation[77]. Kindlin family proteins also participate in integrin activation along with partners such as integrin-linked kinase (ILK) and migfilin. From the many integrin inactivators known to date filamin is the direct inhibitor of integrin activator most studied. It is a rod-shaped protein with 24 immunoglobulin-like domains. Mechanical deformation induces cytoskeleton rearrangements and promotes filamin binding to actin, changing its conformation and revealing new interaction sites[78].

One of the first steps in integrin signaling is FAK recruitment to the β-integrin cytoplasmatic tail[79]. FAK is a target of Src that locates in focal adhesions in a highly phosphorylated state. FAK is incorporated into the focal adhesion by talin and paxilin binding to the C-terminal focal adhesion targeting domain (FAT)[80]. After translocation to the FA, FAK changes its conformation and afterwards, it is autophosphorylated, a state in which it increases Src activity[81]. Src activation increases further FAK phosphorylation and activity. There are several possible FAK regulatory mechanisms: PIP_2 changes near FAs, interactions with Rho GTPases that would affect their activity and localization[82] and also sensitivity to mechanical stress, as fibroblasts devoid of FAK do not show differences in migration directionality in softer or stiffer matrices.

FA are dynamic structures that must be able to alternate between stable and unstable states in rapid response to changes in the environment or intracellular signaling. Forces can modulate the binding affinity of the adhesome by modifying the distance between their bonds (slip bonds) or

exposing new surfaces able to interact with each other (catch bonds)[83]. In that regard, talin acts as both a chemical and mechanical regulator of integrin stability. Talin transmits the pulling force generated by the actin cytoskeleton to integrins, increasing the tension levels of integrin to reach maximum stability (30pN) by a catch bond located in the head of β-integrins. Filamin, in contrast, needs higher forces (40-70pN) to unbind from actin and unfold its immunoglobulin-like domains[84]. Other linker proteins such as kindlin and ILK are almost certain to transmit forces in specific ranges, but mechanical studies have focused on talin so far.

Actomyosin is the main effector involved in reinforcement and dismissal of intracellular tension: myosin contraction modulates tension levels while actin acts as a scaffold for adhesome components and transmits force to the FA. Two independent studies have compared FA composition of fibroblasts seeded on fibronectin before and after blebbistatin mediated myosin-II inhibition[85,86]. Adhesome components close to integrin (talin, kindlin) did not change their composition whereas distant ones like calpain-2 or protein kinase α (PKCα), were lost very quickly. As integrin mature and assemble, several components of the adhesome can bind to actin fibers flowing reawards to the cell center[87] which exert contractile forces. Talin and α-actinin are the main actin couplers while FAK, paxilin and vinculin are less efficient[88]. However, the stiffness of each protein (the amount of force needed to change its conformation) is different in each case. Integrin and talin unfold in respond to soft forces (0.5 pN/nm and 1.5 pN/nm respectively), while α-actinin is less sensitive (1700pN/nm)[43]. Talin may go through stretch–relaxation cycles of 6-16s regulated by vinculin binding[34] while α-actinin is always transmitting actin cytoskeleton force to the FA. Such hierarchy in force sensitivity suggests additional roles for talin apart from being a mere force transmitter.

Therefore, FA stability is regulated by the mechanical forces pulling and pushing them. Talin, vinculin and other adhesome proteins not only act as a scaffolds but also mediate FA mechanical coupling to the actin cytoskeleton and thus, are key factors determining adhesion turnover. Nevertheless, our understanding of these processes is currently deficient and a detailed model of the spatial and temporal dynamics of mechanical signaling is still missing. Yet, advances in fields such as microscopy, computer sciences and cell biology have provided valuable tools to address such questions[5]. While a significant part of our current knowledge about FA comes from fluorescence microscopy, these techniques are not limited to structural information, as light can provide other types of information that need to be considered.

Techniques used in the study of focal adhesions

Fluorescence is a phenomenon produced when a substance absorbs light, part of which is emitted a few nanoseconds later at a higher wavelength. In biology, the first fluorescent protein (GFP, green fluorescent protein) was discovered in the second half of the past century in *Aequorea victoria*[89]. Nowadays, fluorescent-tagged proteins are an indispensable tool in cell biology. Fluorescence microscopy makes it possible to visualize the cellular sublocalization of tagged proteins in fixed and live cells. Images can be acquired over short and long time intervals if phototoxicity is avoided.

Wide-field microscopy

In a wide-field microscope, the whole sample is excited by a light source (tungsten-halogen or mercury lamps), and the resulting image is then captured by a camera. Fluorescent filters are necessary to control emission and excitation paths. Barrier filters block specific wavelengths and are added after the emission source and before the detector to limit the wavelengths emitted or visualized respectively. In addition, dichroic mirrors reflect excitation wavelengths and pass emission wavelengths[90]. A main problem with wide-field microscopy is that fluorescence coming from regions out of focus interferes with the visualized region, resulting in a lower axial resolution (approximately 700nm in contrast with 250nm in the lateral plane). Other techniques such as confocal microscopy can solve this problem at the cost of lower signal or limited axial range.

Confocal microscopy

The axial noise of wide-field microscopes can be reduced using a confocal microscope. All confocal microscopes are based on the same principle: the addition of two sets of pinholes. The first pinhole is added after the excitation laser and is in a conjugate plane (confocal) with another pinhole present right before the detector. In tandem, both pinholes act as a spatial filter restricting the light detected to just one focal plane (**Fig.5A**). That set up allows to image precise optical sections in the axial plane with a resolution of 500nm[91].

Even if in confocal microscopes the noise is greatly reduced; in exchange, the total intensity decreases up to 90-95%. To increase the signal, these microscopes use lasers as light sources and include photomultipliers to detect the emission. Depending on the pinhole configuration, confocal microscopes can be divided into point-scanning and spinning-disk varieties.

- Point-scanning microscopes scan the imaged area in a rectangular pattern (point by point). The laser beam is controlled by two oscillating mirrors governed by galvanometer motors. The region of interest is scanned row by row until the whole image is obtained. Compared to light speed, mirror movement is slow: standard systems can scan an area of 512x512pixels in 250ms[92], but longer times are usual depending of the settings.
- Spinning disk microscopes use two rotating disks with thousands of aligned pinholes arranged in a spiral pattern (**Fig.5B**). The laser crosses the pinholes and excites the sample as in point-scanning but, in this case, the disks spin at high speed, covering the whole area being imaged in only 1ms[93]. In this way, image acquisition is two orders of magnitude faster than point-scanning microscopes and phototoxicity is reduced. There are two main drawbacks of this technique: firstly, the axial depth is fixed, reducing the flexibility when imaging different thicknesses; secondly, due to different distances to the center between central and peripheral pinholes, their linear speed is different and an intensity gradient centered on the middle is formed, as this area is exposed to more photons.

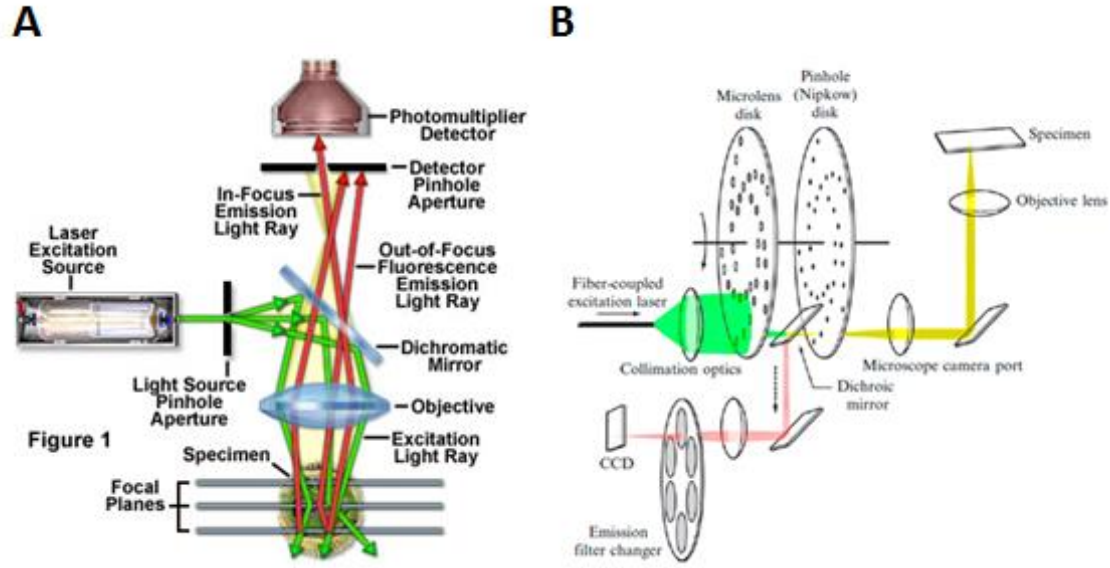

Figure 5. [A] Light paths in confocal microscopy[91]. [B]Design of a spinning disk microscope[93].

10-100nm: Superresolution

Superresolution microscopy is a general term that encompasses an extensive array of techniques capable of obtaining a resolution beneath the refraction limit, reaching values as low as 10nm. Such precision needs of long times of acquisition and potential photobleaching, so superresolution is not yet an optimal choice for live cells. Superresolution microscopy is a technology still in development and, as could be expected, many technical variants coexists nowadays. The main methods can be classified in four broad categories according to their approaches: (i) increase in optical performance

(multiple objectives)[94], (ii) changes in the point spread function[95,96], (iii) iterative localization of single molecules[97–99] and (iv) total internal reflection[100]. Single-molecule localization microscopy has already been used to understand the architecture of FA[28].

Förster resonance energy transfer (FRET)

If the emission spectrum of one fluorophore (donor) overlaps with the excitation spectrum of another (acceptor) and both fluorophores are in close proximity while the donor is excited, part of the energy received by the donor will be transferred to the acceptor, which will emit fluorescence as well (**Fig.6**). This phenomenon is known as Förster resonance energy transfer (FRET)[101]. The amount of energy transfer is usually expressed as FRET efficiency and depends on the Förster radius (R_0), (i.e. the distance at which 50% of the energy is transferred) and the sixth power of the distance between donor and acceptor (r_{DA}):

$$FRET\ eff. = \frac{R_0^6}{R_0^6 + r_{DA}^6}$$

Where R_0 (nm) is a function of the fluorescence quantum yield of the donor (Q_D), the spectral overlap between donor and acceptor (J_{DA}), the refractive index of the media (n), the relative angular dispositions of the donor emission and the acceptor absorption dipole moments (k^2), and C, a constant ($8.79 \cdot 10^{-11}$M·cm·nm^2):

$$R_0^6 = 8.79 \cdot 10^{-11} \cdot [Q_D \cdot k^2 \cdot n^{-4} \cdot J_{DA}]$$

Because of the term including the sixth power of the distance, FRET is only observed at less than 10nm between the FRET pair, and offers sensitive information about proximity below the resolution limit of confocal microscopes, acting as a molecular ruler. Because of its properties, FRET is used to assess conformational changes (intramolecular FRET) and analyze the proximity between molecules (intermolecular FRET).

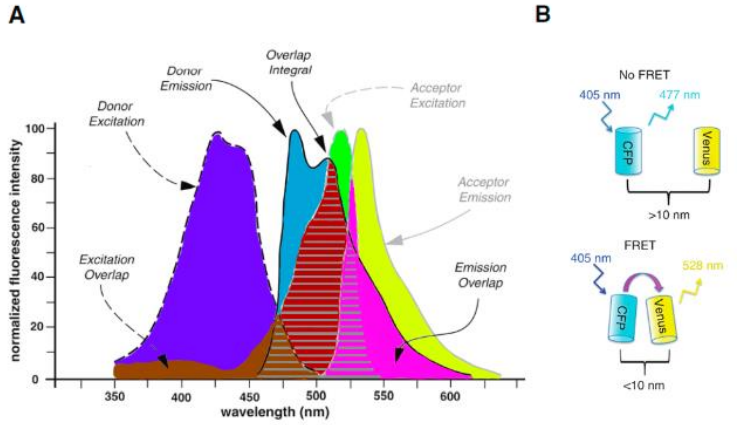

Figure 6. [A] Fluorescent spectra of a FRET pair: CFP (donor) and YFP (acceptor). The brown stripped area corresponds to donor crosstalk, whereas the pink stripped one represents acceptor leakage. The brown area without stripes is a region where homoFRET occurs. The corrected FRET signal measured is represented in red. [B] Principle of FRET[142]. CPF, cyan fluorescent protein. YFP, yellow fluorescent protein.

The overlap between donor emission and acceptor excitation must be high enough to be detected. Despite that, FRET signal is usually low. Besides, it is important to minimize sources of bleed-through such as simultaneous excitation of both fluorophores (acceptor leakage) and emission spectrum in common (donor crosstalk). Furthermore, donor emission and excitation should be as distant as possible to prevent excitation between donors (homoFRET)[102]. Some fluorophore combinations satisfy all these requirements, such as GFP-RFP and CFP-YFP and their variants.

If intermolecular FRET is being measured, the concentrations of donor and acceptor need to be controlled, as the probability of energy transfer increases with higher acceptor/donor ratio. In intramolecular FRET, on the other hand, it is necessary to check possible interactions between FRET pairs of different molecules (unintended intermolecular FRET). Chromatic aberration needs to be corrected as well. Chromatic aberration is an optical distortion produced due to the different refractive index for each wavelength in the same media. As a consequence, not all colors are in the same focal plane and the image obtained shows a false relative displacement between channels. To

solve that problem, such displacement has to be measured, usually imaging multifluorescent beads and aligning the images taken.

While FRET efficiency *per se* is a direct value, it is not measurable on the microscope. Instead, a FRET index is calculated from the images taken. There are several FRET indexes and comparisons between them can be difficult, as each is best suited for specific experimental approaches. (i) Intensity-based FRET quantifies the increase in acceptor emission compared to donor or acceptor intensity; a ratio that is then corrected for bleed-through. (ii) In spectral FRET, the contribution of each fluorophore is calculated by linear unmixing as the spectral properties of the fluorophores are known. That approach requires additional equipment (i.e. a spectral detector)[103] but it makes possible to use FRET pairs with more overlapping spectra (which usually exhibit enhanced FRET). Nonetheless, spectral detectors display low quantum efficiencies[102]. (iii) Other techniques are based on other consequences of FRET such as photobleaching protection[104], changes in fluorescence half-time[105] or light anisotropy[106].

Each FRET method is best suited for the equipment available (microscopes, lasers, filters) and the kind of measurement intended. For simple observations such as FRET change over time or intramolecular FRET (acceptor-donor ratio is always 1:1), it is advisable to start using the simplest intensity-based methods. In contrast, life-time measurements are more appropriate in intermolecular FRET, where probe concentration can be an issue, as those are concentration independent. FRET changes are not necessarily big and, as a consequence, all possible sources of error should be quantified with the right controls such as imaging acceptor or donor only, bleached acceptor or donor, intermolecular controls for intramolecular FRET, etc. Combination of two FRET methods can increase the reliability of the results obtained but, in any case, FRET, as any other technique, should be confirmed by alternative means.

The fact that integrins are found in heterodimers whose conformation changes according to their activation state makes FA attractive targets for FRET. The most relevant FRET approach for this project was the first reported molecular tension sensor, which was used to the force-bearing role of vinculin[62]. The Schwartz laboratory designed a vinculin chimera that incorporated a FRET pair (mTFP1 and venus(A206K)) separated by an elastic spider silk protein flagelliform domain acting as a nanospring[107]: when force was applied to vinculin, the spring became stretched and the distance between fluorophores increased. Those events could be effectively observed by changes in FRET efficiency.

<u>Fluorescence recovery after photobleaching (FRAP)</u>

FRAP is based on the fact that after enough excitation, fluorophores become irreversibly bleached (i.e. their fluorescence is depleted). When a certain spot is bleached in a cell, the resulting area becomes darker, but its intensity changes with time as new, nonbleached molecules diffuse into the dark area until an equilibrium is reached[108]. A fraction of the molecules can be exchanged, allowing to recover fluorescence (mobile fraction), but when part of the population cannot be exchanged (immobile fraction) the original intensity will not be totally recovered. When intensity at each time point after bleaching is compared with the average intensity before bleaching, an exponential FRAP curve ranging from 0 to 1 can be calculated (**Fig.7**), which, fitted, allows to obtain three relevant biophysical parameters.

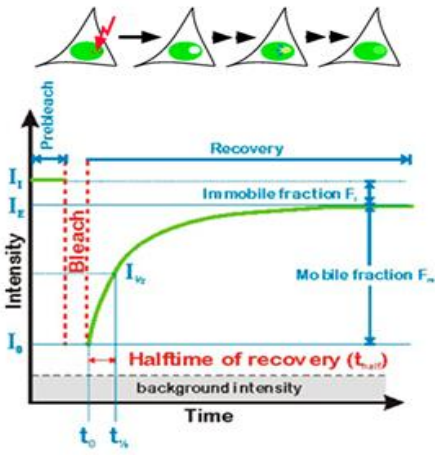

Figure 7. Principle of FRAP[143] and main parameters[144].

- Mobile (Mf) and immobile fractions. Molecules do not exchange freely within cells, they also interact with other binding partners with high and low

affinity. All bleached proteins are eventually replaced, but if such process is slower than the observation, it is possible to calculate immobile and mobile fractions after an arbitrary amount of time.

- Half-time ($t_{1/2}$) and diffusion constant (D). The half-time is the time needed to recover half of the original intensity. $t_{1/2}$ is used to easily calculate the lateral diffusion of membrane proteins when no other recovery is involved and a circular spot is used[109].

There are many practical considerations that must be taken into account when designing a FRAP experiment. Firstly, the fluorescent construct expressed should not interfere with protein function or promote protein aggregation (which is especially relevant in structures such as FA). Besides, a high intensity and intensity range is necessary for precise measurements. More data is obtained with higher acquisition rate but, in return, samples are more prone to photobleaching and photoxicity. It is necessary to archive a compromise between both variables, which will change according to the mobility of each protein.

Mechanical stimuli in live systems

Besides biophysical measurements, it has also been necessary to develop new means to add mechanical perturbations in the biological models used models.

Mechanical forces can be directly applied over cells in a controlled fashion. Flow chambers can simulate the shear forces exerted in the vascular endothelium and the lymphatic system[110]: cells are seeded in a chamber whose media is being pumped. Additionally, mechanical stretchers exert compression and extension forces[111]. In that case, cells are seeded on a membrane made of biocompatible, transparent materials, which is then stretched mechanically or using vacuum. As the membrane area increases, the force is transmitted to cells, which can be observed during and after the process.

Translation of biomechanical findings into animal models is difficult. In vascular biology, the aorta can be used to observe differential responses to mechanical stimuli. While flow in the ascending aorta resembles a turbulent regime (it is closer to the left ventricle), the descending aorta resembles a laminar flow[112], giving rise to different shear forces. Inducing an increase in blood pressure (pregnancy, renin-angiotensin system) can be another way to exert changes in the mechanical environment of the organism studied.

Small molecules able to inhibit actomyosin contractibility are an extended tool in mechanotransduction. While siRNA can be used to deplete myosin II, drugs offer a faster and precise alternative[113]. The compounds used in the experimental part of work project are commented next (**Fig.8**).

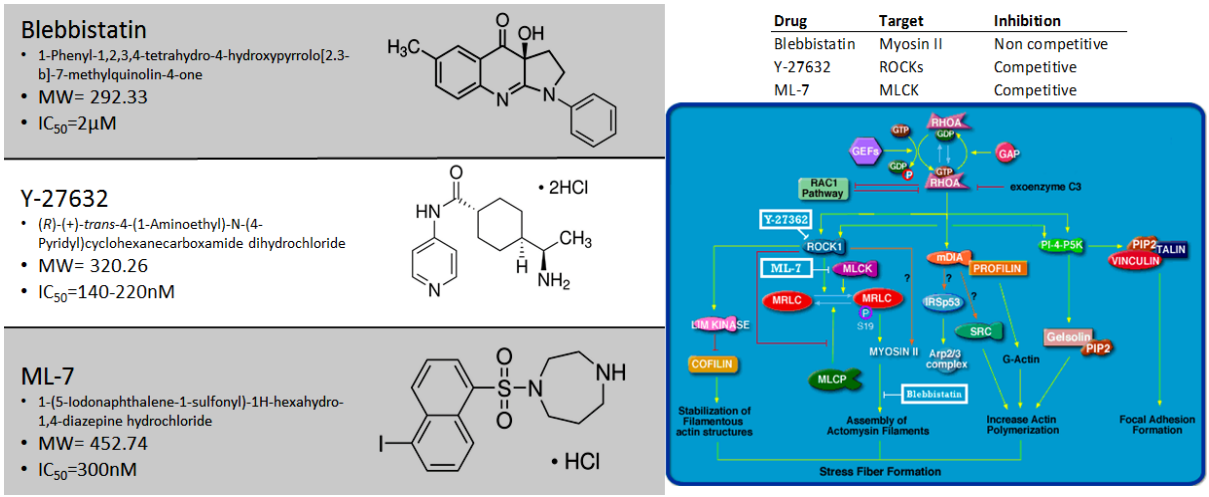

Figure 8. Inhibitors of actomyosin contractibility used in this work. Left: Chemical properties[120]. Right: Inhibitory mechanisms[141].

Blebbistatin is the most widely used inhibitor of non-muscle myosin II. It is a noncompetitive inhibitor that binds the motor domain by hydrophobic interactions, resulting in the stabilization of the pre-power stroke state (myosin associated with ADP and Pi, but not actin) and the inhibition of Pi release[114]. This is a very specific compound: while it has IC_{50} of 2µM it does not hinder myosin I or V and concentrations as high as 50µM. Blebbistatin is highly permeable, acts fast and its effects are reversible but, in contrast, has low solubility and is inactivated by high levels of blue light (below 488nm)[115]. A derivative of blebbistatin, azidoblebbistatin, does not present these drawbacks but, in exchange, needs to be irreversibly photo-crosslinked with myosin using ultraviolet light[116].

Y-27632 is a Rho-associated protein kinase inhibitor. The ROCK family comprises ROCK-I (p160ROCK) and ROCK-II (also known as ROKα or Rho-kinase). This Y-compound acts by competitive inhibition and prevents the use to ATP by ROCKs[117]. Addition of Y-27632 unsets the balance in MLC phosphorylation as it inhibits myosin phosphatase and may phosphorylate the myosin light chain directly. The IC_{50} of Y-28632 is 140-220nM[118] .

ML-7 is a competitive MLCK inhibitor that prevents MLCK binding to ATP. The effects of ML-7 and Y-27632 may be spatially regulated: ROCK activity is necessary for actin stress fibers formation in the center of the cells, whereas MLCK is required for peripheral MLC phosphorylation [119]. ML-7 IC_{50} is 300nM [120].

Objectives

Despite the evidences hinting at the role of talin in mechanotransduction, a direct assessment of the forces borne by that protein is still missing. In this work, we continued the approach started in the Schwartz laboratory and used a novel talin force sensor (TS) and FRET microscopy to examine the role of actomyosin contractibility in talin tension. FRET tension sensors need precise measurements, so the suitability of the experimental design had to be tested in biological and microscopy terms before extracting valid conclusions. Talin binds integrins and actin directly. Consequently, we expected to observe a dismissal in the tension suffered by talin once its interaction with actin was prevented or actomyosin contractile forces were reduced. The objectives of this work can be summarized as:

1. Dissect the sources of error in FRET measurements in talin tension biosensors and correct them.
2. Describe the differences between TS and wild-type talin in biophysical terms.
3. If the use of TS is a valid approach for tension measurements, study the role of actomyosin contractibility on the forces being exerted on talin.

Results

Tension measurements require stringent calibration

Several constructs featuring the tension sensor module in talin were designed (**Fig.9B**). (i) TS (talin sensor): with the tension module fused in the linker domain; (ii) NTS (N-terminal talin sensor), where the FRET pair is in the N-terminus, and it should not experience forces able to separate the fluorophores; (iii) GT (eGFP (enhanced GFP) -talin), in which only GFP and not the rest of the module was fused into the N-terminus, and (iv) TA (mutated ABS talin sensor), identical to TS except in its C-terminal actin binding site (ABS), which was mutated to prevent actin binding. These constructs were transiently transfected in Talin-1 KO 3T3 mouse fibroblasts for FRET studies. That cell line only expressed talin-1 at very low levels, but it retained wild-type expression levels for talin-2 (data not shown).

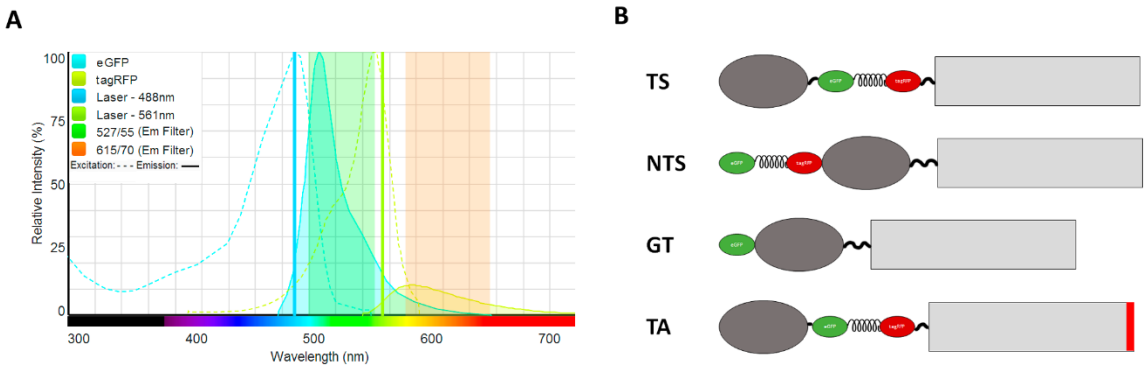

Fig.9. [A] Spectral overlap between eGFP and tagRFP. Dotted lines represent the excitation spectra of both fluorophores, and continuous lines, the emission spectra. The bold lines indicate the lasers used for FRET imaging, while the colored areas represent the filters used to detect donor emission (blue) and acceptor emission (orange). [B] Talin tension sensor constructs used in this work, described in the text. eGFP is represented in green and, tagRFP, In red. Talin head domain is in dark grey and the rod domain in light grey.

To reduce phototoxicity and speed up acquisition times, spinning disk confocal microscopy was used as imaging system. eGFP[121] and tagRFP[122] were chosen as FRET pair because they present a considerable overlap in donor emission and acceptor excitation (**Fig.9A**) and they could be excited with the equipment available. Sources of error in FRET imaging were analyzed and corrected. Previously, intermolecular FRET had been calculated cotransfecting talin-1 KO 3T3 mouse fibroblasts

with mutated versions of TS where only one the fluorophores was active. FRET values obtained represented a 5% of the efficiency normally observed with TS in spread cells (data not shown).

To correct for fluorescence bleed-through, 3T3 mouse fibroblasts were transfected with either eGFP or tagRFP and imaged in eGFP, FRET (eGFP excitation, tagRFP emission) and tagRFP channels. The linear dependency between intensity and bleed-through was then calculated. It was constantly around values of 4.5-5% for donor crosstalk and 6-8% for acceptor leakage. Due to instrumentation limitations, homoFRET could not be analyzed.

Confocal microscopy is sensitive to chromatic aberration. The objectives used were Apochromat, through a displacement of one pixel between channels was observed at the highest magnification (100x) with multifluorescent beads and corrected. The intensity gradient in spinning disk microscopes was quantified imaging fluorescent dyes: the differences observed were, at the image borders, 50% lower compared to the center.

In order to assess the impact of these calibration procedures on FRET efficiency, FRET values were compared in the same cell with and without the corrections in use. Lack of calibration, especially bleed-through, led to a drastic increase in FRET efficiency (**Fig.10**).

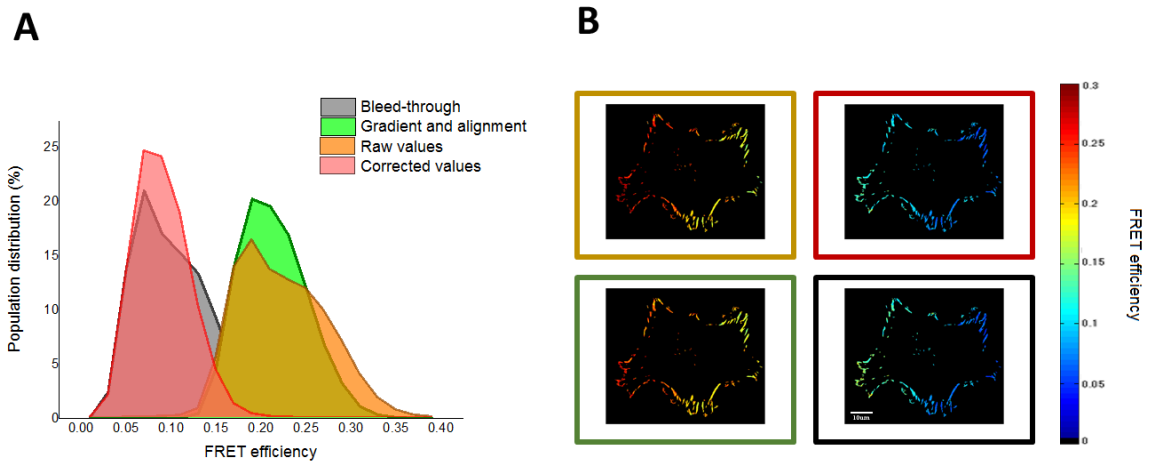

Figure 10. [A] FRET efficiency distribution at focal adhesion after applying some or all corrections necessary. As can be observed, bleed-through correction had the strongest impact in FRET index. [B] FRET images with or without correction. The frame colors indicate the same correction that in [A]. All images in this project use the same FRET color scale (0.0-0.3) that this figure. Bar = 10µm.

Actomyosin inhibitors exert differential effects on talin tension

To check whether talin tension was actually being measured in TS, we compared FRET values between talin present at FA and the cytoplasm (**Fig.11A**). Higher FRET values were detected in the cytoplasmic pool. These differences were also present in regions close to the plasma membrane but outside FA in comparison with talin in FA themselves.

To directly address the role of contractile forces, actomyosin contractiblity was inhibited using small molecules (**Fig.11B**). With that purpose, FRET efficiency was measured in FA in random fixed cells after treatment with vehicle (DMSO) or three reversible inhibitors at two concentrations (5µM and 10µM): blebbistatin (myosin II inhibitor), ML-7 (MLCK inhibitor) and Y-27632 (ROCKs inhibitor) (**Fig.8**). At high doses (50µM), these compounds led to aberrant cell shape and loss of membrane rigidity, a property that was used as a positive control to check drug stability (**Fig.11C**). As we wanted to observe the subtle effects of a decrease in actomyosin pulling force, lower doses of 5µM and 10µM were used. To discard any other effect on FRET efficiency besides actin stretching, the assay was also performed with NTS, which showed higher baseline FRET values. DMSO treatment still presented significant differences between NTS and TS FRET efficiency, whereas FRET increased in TS after blebbistatin addition and high doses of ML-7. On the other hand, no changes were observed upon Y-27632 treatment or a combination of ML-7 and Y-27632. Strikingly, FRET decreased in a constant

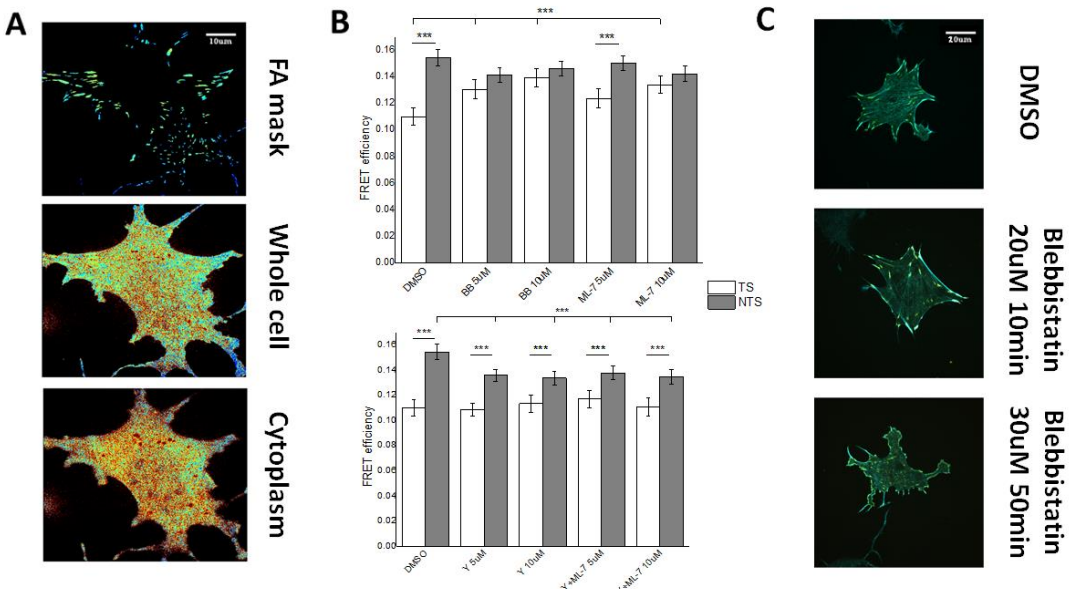

Figure 11. [A] FRET efficiency values in focal adhesions, the whole region close to the plasma membrane and the cytoplasmic pool of talin respectively. [B] Mean pixel FRET values in focal adhesions after chemical disruption of actomyosin contractibility. (***) indicates values statistically significant ($p<0.001$, $d>0.5$). [C] Effect of high and moderate doses of blebbistatin on cytoskeleton integrity. Green, Talin sensor; blue, Alexa Fluor 647 phalloidin. DMSO, dimethyl sulfoxide.; TS, talin sensor; NTS, N-terminal talin sensor; BB, blebbistatin; Y, Y-27632. Bar: 10µm

fashion in NTS after all treatments but DMSO. These inconsistencies led us to consider a further characterization of TS compared to wild-type talin as well as a more detailed study of which additional factors could be affecting FRET efficiency with the methodology used.

Evaluation of fixation and diffusion effects on FRET

The role on paraformaldehyde (PFA) in FRET efficiency was analyzed imaging the same cells at different stages before and after fixation (**Fig.12**). Surprisingly, a drastic reduction in fluorescence intensity as high as 50% was detected (data not shown) and a simultaneous decrease in FRET efficiency short after fixation and consequent washing steps. 24 hours later, FRET and raw intensity partially recovered to 60% of their former values.

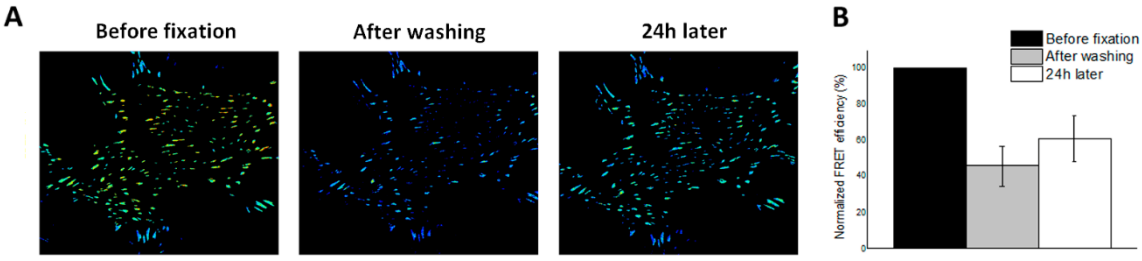

Figure 12. [A] FRET values at focal adhesions of a representative cells during the fixation process. [B] Relative changes in FRET efficiency observed on individual monitored cells. Both values are statistically significant ($p<0.001$).

FRAP assays were performed on TS and GT (endogenous talin cannot be used as FRAP requires necessarily a fluorescent protein) to detect possible differences in their kinetics that could affect live experiments (**Fig.13**). A circular region of 0.3µm in radius was bleached in the eGFP channel to around 40-50% its former intensity value. Cells were then imaged every 3 seconds in eGFP channel for 5 minutes.

Significant differences could still be observed between TS and GT both in their recovery rates and mobile fractions. In fact, recovery was slower but archived a higher value in GT (62.4% of corrected original intensity versus 39.5%). These parameters made possible to obtain the diffusion constant of

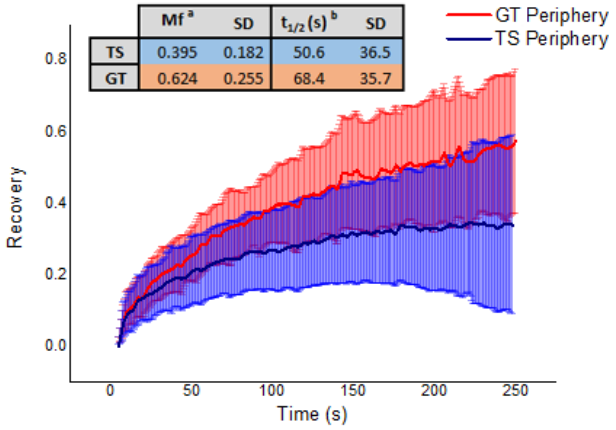

Figure 13. [A] FRET values at focal adhesions of a representative cells during the fixation process. [B] Relative changes in FRET efficiency observed on individual monitored cells. *a* and *b* were both statistically significant between groups ($p<0.001$).

each construct: $D_{TS}=5.31\cdot10^{-12} \pm 25.7$ % cm^2s^{-1} while $D_{GT}=2.96\cdot10^{-12} \pm 18.4$ % cm^2s^{-1}. Contrary to what could be expected by their size, TS presented higher diffusivity. Nonetheless, despite the statistical significance of these differences, some cells could have been experiencing phototoxicity. Overall, TS kinetics were considered equivalent to GT.

Live FRET imaging after actomyosin contractivility inhibition

To study the role of direct talin-actin interactions in force transmission, we performed live FRET experiments in talin-1 KO fibroblasts transiently expressing with TS or TA. Cell were treated with the drug and dose with the strongest effect (blebbistatin 10µM) and images were acquired before drug addition and at 5 minute intervals after the treatment (**Fig.14**). Changes in untreated TS cells were minimal, while blebbistatin induced an increase in FRET efficiency after 25 minutes. FA started to disappear and in some cases cell integrity became suddenly compromised (**Movies S1 and S2**). On the other hand, untreated TA transfected cells presented higher baseline FRET efficiency, close to NTS values in fixed samples (data not shown), and they were not affected by contractility inhibition.

Discussion

FRET as a tool for tension measurements

FRET can be affected by several factors such spectral overlap, light out of focus and the refractive index[123]. In the methods presented here, we have detected and corrected such sources of error. PFA fixation is known to affect fluorescence life-time and FRET efficiency for the CYP-YFP pair[124,125] but those effects have not been reported for GFP[126]. However, due to the high similarity between fluorescent proteins (YFP is in fact a GFP T203Y mutant[127]), our results could not exclude such possibility. Besides, PFA is a fixative agent that cross-links proteins forming methylene bridges[128] while other components such as lipids and sugars are trapped in the resulting insoluble matrix. Those changes, together with the higher viscosity of PFA (20cP) compared to water (1cP) may have resulted in a loss in fluorophore rotational freedom that could lower FRET efficiency. It has been previously reported that

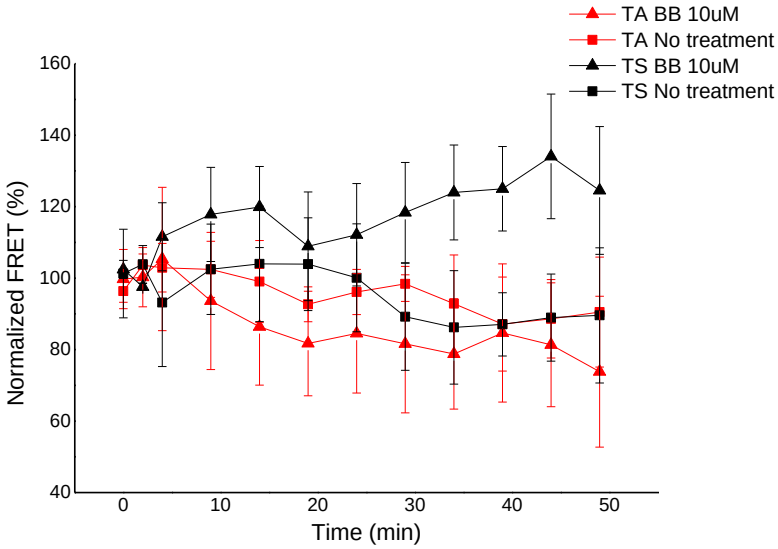

Figure 14. Normalized Changes in FRET efficiency after blebbistatin treatment. BB, Blebbistatin; TS, Talin sensor; TA, C-terminal actin binding site mutant talin sensor.

mechanosensitivity of focal adhesions depends greatly on pH[129], so small changes in PFA acidity between experiments could also be present in this work and should be addressed in the future. The addition of new control sensors with different elastic properties and changes in the localization of the tension sensor module should also be considered. The cell line used, talin KO mouse 3T3 fibroblasts, still expressed *Tln2* and very low levels of *Tln1,* but in contrast to endothelial cells, which only express *Tln1*, they are physiologically exposed to a wider range of forces (in the range of 30-200nN [130]) and, consequently, offered a bigger window for analysis.

Our FRAP results should be interpreted cautiously. In contrast to previous reports[131], we could not compare kinetics between FA located in the periphery and the center of cells: bleached central FA presented low signal to noise ratios and their lifespan was in some cases shorter that the total interval analysed, they were discarded from further analysis. Besides, some cells presented spontaneous contraction, a symptom of phototoxicity probably due to the frequency of image acquisition, and they were also removed from our dataset. Despite those confounding factors, we could observe differences in kinetics between fluorescent constructs. The size of TS and GT is equivalent (3056 residues compared to 2779) so diffusivity differences might be caused by conformational changes affecting binding affinity with other molecules. Previous FRAP studies of talin showed great differences with half-times as diverse as 77s, 50s, 4.51-6.82s[132] or even 2.2s[131] The FRAP values reported here are consistent between both constructs and they are closer to those obtained from mouse embrionary fibroblasts in the literature (50s, 62s)[133]. In another FRAP study, the mobile fraction is similar to the one obtained here (55%) while the half-time was significantly lower (17s). These divergences in FRAP parameters could be due to differences in the cell line used as well as bleaching settings and mathematical models used. In both cases, however, the diffusion coefficients were similar to those of other slow membrane proteins[109], which present values around in the order of 10^{-10}-10^{-12} $cm^2 \cdot s^{-1}$ instead of cytoplasmic proteins such as GFP ($2.5 \cdot 10^{-9}$) $cm^2 \cdot s^{-1}$. That fact suggests that the main factor in intensity recovery it is not the cytoplasmic pool, but other talin molecules present in the FA.

Talin mechanosensitivity depends on direct actin interaction

FRET requires a deep understanding of its biological and physical implications: measurements need to be meticulously taken and the effect on the tension module should be analysed for each protein. Despite such limitations, a recent study also incorporated a new FRET tension sensor on PECAM-1 (platelet endothelial cell adhesion molecule 1) to analyze the effect of shear stress on PECAM-1 tension[134]. Both for that sensor and the vinculin one, the results obtained by FRET challenged part of the current assumptions in the field (force dependent recruitment of vinculin and absence of cytoskeleton reorganization after shear stress respectively), prompting new interesting questions to be asked.

In the current model, talin is activated at the plasma membrane after PIPK1γ90 mediated recruitment, followed by force dependent stretching and changes in binding affinity[20]. So far, the only direct evidences for a mechanical regulation of talin were provided by studies based on magnetic beads and optical tweezers[43]. Here we report the use of a biosensor to measure tension across talin directly on cells. We found that tension was reduced in the cytoplasmic pool and in membrane-proximal talin outside focal adhesions and that actomyosin contraction inhibition by small molecules decreased the mechanical load of talin but those effects were notably reduced when the C-terminal ABS was mutated.

Differences in drug treatments can be conciliated. MLCK acts upstream myosin II[113] and therefore, the presence of compensatory mechanisms after ML-7 addition is more feasible than in blebbistatin treatment. An increase in MLCP or ROCK activity could be behind the higher dose of ML-7 necessary to observe effects. These changes could be mediated by fast posttranslational modifications catalyzed by other proteins of the adhesome, like the multiple kinases present in FA[135]. At the same time, ML-7 mediated decrease in ROCK activity could have been compensated by a simultaneous decrease in Rac1

mediated RhoA inhibition. Besides, ROCK is especially necessary for actin polymerization in the cell center, whereas MLCK is required for peripheral actin contraction. As most of the FAs measured were in the periphery, Y-27362 effect could have been effectively masked. A refinement in the algorithm used to identify FA would be needed to address that question.

Despite the diverse talin binding partners able to associate with actin (vinculin, FAK)[32], tension values in TA were similar to NTS (albeit in fixed samples), reinforcing the importance of direct interactions with the cytoskeleton network in force transmission and generation. In future work, it would be interesting to relate the changes in talin tension during cellular processes such as migration or spreading and the role of additional molecular interactions with other adhesome proteins using additional mutant sensors.

Conclusion

Overall, this work has characterized tension biosensor based on FRET as a multidisciplinary approach to assess the role of forces at cellular and molecular levels, providing new evidences about the function of actomyosin in talin mechanosensitivity regulation.

Here, we have demonstrated that a direct link between actin and talin is necessary for the transmission of physical force started by myosin contraction. Such evidence will surely constitute the first step in the biomechanical characterization of talin.

Materials and methods

Cell culture and transfection

Talin-1 KO 3T3 mouse fibroblasts were cultured in Dulbecco's modified Eagle's medium (DMEM) containing 10% fetal bovine serum (FBS), 0.001% β-mercaptoethanol (Sigma, US) and 1.2mg/ml $NaHCO_3$ (Sigma, US) Cells were cultured in a 5% CO_2 humidified atmosphere at 37ºC and supplemented with penicillin-streptomycin, which was removed from the medium before and during experiments.

Cells were seeded in a 6-well plate and transfected with jetPrime (Polyplus Transfection, US) with 1µg of the construct at 50-60% confluence. After 24h, an efficiency of 50% was observed by wide field microscopy. For further analysis, 48h after transfection, cells were lifted with trypsin and plated on glass bottom dishes (⌀20mm) coated with fibronectin (10mg/ml) for 3h at low confluence (35.000cells/well) to allow spreading and formation of FAs. The constructs used in this work were: eGFP, tagRFP, GT, TS, NTS and TA.

Drug treatments and immunostaining

Following transfection and subsequent spreading, cells were incubated with two concentrations (5µM or 10µ M) of blebbistatin (diluted in DMSO), Y-27632 (diluted in DMSO), ML-7 (diluted in water) or combinations of the aforementioned. Fibroblasts treated with the vehicle (DMSO) only were used as negative control, whereas incubation in blebbistatin 30µM for 50 minutes was used as positive control. Cells were used for live imaging or fixed with PFA 4% (prepared from powder (Sigma)) for 20 minutes. To measure global changes, random cells were imaged before and after incubation for 10, 20 or 50 minutes and posterior fixation. To monitor individual cells, time-lapse image acquisition was performed right before incubation and at 5 minute intervals after drug addition for as long as 45 minutes. For immunostaining, samples were permeabilized with Triton X-100 0.1% (Sigma) and fixed using PFA 4%. Incubation for 20 minutes with Alexa Fluor 647 phalloidin (Live sciences) was carried out for actin visualization, as this fluorophore did not overlap with the FRET pair emission spectra.

Image acquisition and calibration

FRET experiments were conducted using a Nikon Eclipse Ti spinning disk microscope (Nikon) with a Nikon Plan Apochromat x100 NA=1.4 objective or a Nikon Plan Apochromat x60 NA=1.4 objective. The microscope was controlled by Volocity software (Perkin Elmer). Three laser lines were used (488nm, 561nm and 640nm) altogether with 3 band filters for eGFP emission (499.5-554.5nm), tagRFP emission (580-650nm) and Alexa Fluor 647 emission (660-750nm). All images were taken with the same settings: 10% laser power and exposure time of 500ms for FRET experiments and 10% laser power with 100ms of exposure time for FRAP experiments. FRET efficient values were similar in fixed and live samples. Therefore, the effect of fluorophore diffusion during the acquisition interval and its impact in FRET efficiency was not further considered. For FRAP experiments, an UltraView Photokinetic unit (Nikon) was used.

To correct images for intensity gradients, samples with solutions of synthetic dyes equivalent to the fluorophores used (Atto488 for eGFP and Atto565 for tagRFP (Atto-TEC, US))) were imaged. The background from each image was estimated as the average intensity in the channel devoid of fluorophore and subtracted. The resulting intensity was normalized by the maximum intensity value, obtaining a [0,1] matrix for each fluorophore used to correct the rest of the pictures. For FRET images, the donor gradient was used. Alignment between channels was checked periodically using multifluorescent beads of 0.2µm of diameter. (TetraSpeck™ Fluorescent Microspheres Size Kit, Life Technologies). In the 60x objective, no chromic aberration was observed, whereas the 100x objective showed a relative displacement of 1 pixel between channels.

In FRAP experiments, to correct the alignment between the area selected and the region actually bleached by the photobleaching device, a fluorescent painted sample was used. For FRET imaging, bleed-through correction was performed imaging monolabeled samples (wild-type 3T3 fibroblasts transfected with eGFP or tagRFP) with both the corresponding fluorophore and FRET. Smooth nuclear regions of interest were cropped and analyzed with Matlab to calculate the percentage of donor leakage and acceptor cross-talk (*d* and *a* respectively). eGFP and tagRFP pixel values were plotted against FRET and the values were linearly fitted: donor leakage usually ranged between 4.5-5% and acceptor crosstalk between 6-8%. The required calibrations were done for each imaging session.

Föster Resonance Energy Transfer (FRET) assays

There are several methods to quantify FRET efficiency. In this case, intramolecular FRET was being measured and 1:1 ratio between donor and acceptor was assured, so a simple ratiometric intensity-based FRET index was chosen. Intensity was normalized using the acceptor channel by:

$$FRET\ eff. = \frac{I_{DA} - aI_{AA} - dI_{DD}}{I_{AA}}$$

Where I_{DA} represents the intensity produced when exciting at the donor (D) excitation spectrum and measured in the acceptor (A) emission spectrum; while *a* and *d* are constants obtained experimentally that describe the linear dependency between intensity and bleed-through.

Raw images were analyzed with Matlab 2012a (MathWorks). Background intensity was subtracted from all images using the mean values of a region void of cells manually selected for each picture. Calibrations were incorporated into the script in the following fashion: (i) images were divided by a matrix with the values of relative intensity obtained with gradient correction and, in the case of FRET channel, donor gradient was used, (ii) the relative position of each channel was modified according to the bead alignment results, (iii) FRET efficiency was calculated for each pixel using information from the three corrected channels and the bleed-through coefficients obtained experimentally. FRET values were smoothed to remove potential artifacts.

FRET values were filtered to just select FA. For FA segmentation, a mean background value was obtained and only pixels above 110% that intensity in the eGFP channel were further considered. Despite the higher autofluorescence of eGFP compared to tagRFP, eGFP was chosen for segmentation

as it did not present as many fluorescent vacuoles as tagRFP. Next, a blur filter was applied and intensities above Mean+0.75Sd (standard deviation) were considered of interest: continuous regions of 25 or more pixels were identified as FAs and used as masks.

To quantify FRET changes within the same cell after treatments, we used a normalized FRET percentage in FA:

$$Normalized\ FRET = \frac{100 \cdot\ Mean\ FRET}{Mean\ FRET\ before\ treatment}$$

Fluorescence Recovery After Photobleaching (FRAP) assays

FRAP assays were conducted on talin-1 KO 3T3 fibroblasts expressing either TS or GT. Samples were imaged at 37ºC in DMEM supplemented as previously described. Bleaching was carried out at a wavelength of 488nm at 100% laser power on several spots of 0.6µm of diameter at the same time. Spot intensities were reduced to 40-50% of their original values, as more bleaching led to increased phototoxicity. Cells were imaged for eGFP at 1 frame per second for 5 seconds before bleaching (frames 1-5) and every 3 seconds for 5 minutes afterwards (frames 6-305).

Background (Bk), bleached FAs (Bfa) and non-bleached FAs (Cfa) regions were manually selected with ImageJ[136], adjusted frame by frame to track their movement and their mean intensity measured. Double normalization[137] was used to calculate FRAP recovery curves and an average of 3 Cfa were selected to normalize for bleaching during image acquisition. To adjust FRAP curve to a range from 0 to 1, recovery right after bleaching was assigned a value of 0 by the following expression

$$Recovery = \frac{Bfa'_{(i)} - Bfa'_{(6)}}{Bfa_{(mean\ 1-5)} - Bk_{(mean)}}$$

Where

$$Bfa'_{(i)} = Bfa_{(i)} \cdot \frac{Cfa_{(mean\ 1-5)} - Bk_{(mean)}}{Cfa_{(i)} - Bk_{(mean)}}$$

The resulting data was fitted into a monoexponential function. Half-time ($t_{1/2}$) and mobile fraction (Mf) were calculated for each construct according to the equation

$$Recovery = Mf\left(1 - e^{-\tau \cdot t}\right)$$

Where

$$\tau = \frac{ln0.5}{t_{1/2}}$$

Diffusion coefficients were calculated using the Kapitza method[138]:

$$D = \frac{\omega^2 ln2}{4 \cdot t_{1/2}}$$

Where ω is the radius of the bleached area.

Statistical Analysis

Statistical analysis and data fitting were performed with OriginPro 9.0 (OriginLab). Data are presented as Mean±standard deviation (SD). Comparison between groups were performed with 2-sample t tests. Differences were considered significant when $p<0.001$ and Cohen's $d>0.5$.

Supplementary material

Movie S1. Time-lapse movie of FRET efficacy after blebbistatin addition (final concentration 10µM). Images were acquired every five minutes. Blebbistatin was added after the first two frames.

Movie S2. Time-lapse movie of eGFP channel after blebbistatin addition (final concentration 10µM). Images were acquired every five minutes. Blebbistatin was added after the first two frames.

References

1. Engler, A. J., Sen, S., Sweeney, H. L. & Discher, D. E. Matrix elasticity directs stem cell lineage specification. *Cell* **126,** 677–89 (2006).
2. Wozniak, M. a & Chen, C. S. Mechanotransduction in development: a growing role for contractility. *Nat. Rev. Mol. Cell Biol.* **10,** 34–43 (2009).
3. Ridley, A. J. *et al.* Cell migration: integrating signals from front to back. *Science* **302,** 1704–9 (2003).
4. Westerhof, N., Stergiopulos, N. & Noble, M. I. M. Snapshots of Hemodynamics. 2nd Ed. 197–205. Springer. New York. (2005).
5. Ingber, D. E. Cellular mechanotransduction : putting all the pieces together again. *FASEB J.* **20**, 811–827 (2006).
6. Kim, D.-H. & Wirtz, D. Focal adhesion size uniquely predicts cell migration. *FASEB J.* **27,** 1351–61 (2013).
7. Zaidel-Bar, R., Itzkovitz, S., Ma'ayan, A., Iyengar, R. & Geiger, B. Functional atlas of the integrin adhesome. *Nat. Cell Biol.* **9,** 858–67 (2007).
8. Schwartz, M. A. Integrins and extracellular matrix in mechanotransduction. *Cold Spring Harb. Perspect. Biol.* **2,** 1–13 (2010).
9. Bouvard, D., Pouwels, J., De Franceschi, N. & Ivaska, J. Integrin inactivators: balancing cellular functions in vitro and in vivo. *Nat. Rev. Mol. Cell Biol.* **14,** 430–42 (2013).
10. Campbell, I. D. & Humphries, M. J. Integrin structure, activation, and interactions. *Cold Spring Harb. Perspect. Biol.* **3,** 1–14 (2011).
11. Burridge, K. & Connell, L. A new protein of adhesion plaques and ruffling membranes. *J. Cell Biol.* **97,** 359–67 (1983).
12. Debrand, E. *et al.* Mice carrying a complete deletion of the talin2 coding sequence are viable and fertile. *Biochem. Biophys. Res. Commun.* **426,** 190–5 (2012).
13. Petrich, B. G. *et al.* Talin is required for integrin-mediated platelet function in hemostasis and thrombosis. *J. Exp. Med.* **204,** 3103–11 (2007).
14. Praekelt, U. *et al.* New isoform-specific monoclonal antibodies reveal different sub-cellular localisations for talin1 and talin2. *Eur. J. Cell Biol.* **91,** 180–91 (2012).
15. Wegener, K. L. *et al.* Structural basis for the interaction between the cytoplasmic domain of the hyaluronate receptor layilin and the talin F3 subdomain. *J. Mol. Biol.* **382,** 112–26 (2008).
16. Goult, B. T. *et al.* Structure of a double ubiquitin-like domain in the talin head: a role in integrin activation. *EMBO J.* **29,** 1069–80 (2010).
17. Ratnikov, B. *et al.* Talin phosphorylation sites mapped by mass spectrometry. *J. Cell Sci.* **118,** 4921–3 (2005).
18. Bate, N. *et al.* Talin contains a C-terminal calpain2 cleavage site important in focal adhesion dynamics. *PLoS One* **7,** e34461 (2012).
19. Critchley, D. R. & Gingras, A. R. Talin at a glance. *J. Cell Sci.* **121,** 1345–7 (2008).
20. Critchley, D. R. Biochemical and structural properties of the integrin-associated cytoskeletal protein talin. *Annu. Rev. Biophys.* **38,** 235–54 (2009).
21. Sun, N., Critchley, D. R., Paulin, D., Li, Z. & Robson, R. M. Identification of a repeated domain within mammalian alpha-synemin that interacts directly with talin. *Exp. Cell Res.* **314,** 1839–49 (2008).
22. Kim, M., Carman, C. V & Springer, T. a. Bidirectional transmembrane signaling by cytoplasmic domain separation in integrins. *Science* **301,** 1720–5 (2003).
23. Diaz-Gonzalez, F. Breaking the Integrin Hinge. *J. Biol. Chem.* **271,** 6571–6574 (1996).
24. Campbell, I. D. & Ginsberg, M. H. The talin-tail interaction places integrin activation on FERM ground. *Trends Biochem. Sci.* **29,** 429–35 (2004).
25. Wegener, K. L. *et al.* Structural basis of integrin activation by talin. *Cell* **128,** 171–82 (2007).
26. Calderwood, D. a *et al.* Integrin beta cytoplasmic domain interactions with phosphotyrosine-binding domains: a structural prototype for diversity in integrin signaling. *Proc. Natl. Acad. Sci. U. S. A.* **100,** 2272–7 (2003).
27. Parsons, M., Messent, A. J., Humphries, J. D., Deakin, N. O. & Humphries, M. J. Quantification of integrin receptor agonism by fluorescence lifetime imaging. *J. Cell Sci.* **121,** 265–71 (2008).
28. Kanchanawong, P. *et al.* Nanoscale architecture of integrin-based cell adhesions. *Nature* **468,** 580–4 (2010).
29. Franco, S. J. *et al.* Calpain-mediated proteolysis of talin regulates adhesion dynamics. *Nat. Cell Biol.* **6,** 977–83 (2004).
30. Huang, C. *et al.* Talin phosphorylation by Cdk5 regulates Smurf1-mediated talin head ubiquitylation and cell migration. *Nat. Cell Biol.* **11,** 624–30 (2009).

31. Zhang, X. *et al.* Talin depletion reveals independence of initial cell spreading from integrin activation and traction. *Nat. Cell Biol.* **10,** 1062–8 (2008).
32. Gingras, A. R. *et al.* The structure of the C-terminal actin-binding domain of talin. *EMBO J.* **27,** 458–69 (2008).
33. Goksoy, E. *et al.* Structural basis for the autoinhibition of talin in regulating integrin activation. *Mol. Cell* **31,** 124–33 (2008).
34. Margadant, F. *et al.* Mechanotransduction in vivo by repeated talin stretch-relaxation events depends upon vinculin. *PLoS Biol.* **9,** e1001223 (2011).
35. Lawson, C. *et al.* FAK promotes recruitment of talin to nascent adhesions to control cell motility. *J. Cell Biol.* **196,** 223–32 (2012).
36. Di Paolo, G. *et al.* Recruitment and regulation of phosphatidylinositol phosphate kinase type 1 gamma by the FERM domain of talin. *Nature* **420,** 85–9 (2002).
37. Ziegler, W. H., Liddington, R. C. & Critchley, D. R. The structure and regulation of vinculin. *Trends Cell Biol.* **16,** 453–60 (2006).
38. Patel, B. *et al.* The activity of the vinculin binding sites in talin is influenced by the stability of the helical bundles that make up the talin rod. *J. Biol. Chem.* **281,** 7458–67 (2006).
39. Goult, B. T. *et al.* RIAM and vinculin binding to talin are mutually exclusive and regulate adhesion assembly and turnover. *J. Biol. Chem.* **288,** 8238–49 (2013).
40. Calderwood, D. a, Campbell, I. D. & Critchley, D. R. Talins and kindlins: partners in integrin-mediated adhesion. *Nat. Rev. Mol. Cell Biol.* **14,** 503–17 (2013).
41. Roca-Cusachs, P., Iskratsch, T. & Sheetz, M. P. Finding the weakest link: exploring integrin-mediated mechanical molecular pathways. *J. Cell Sci.* **125,** 3025–38 (2012).
42. Kong, F., García, A. J., Mould, a P., Humphries, M. J. & Zhu, C. Demonstration of catch bonds between an integrin and its ligand. *J. Cell Biol.* **185,** 1275–84 (2009).
43. Rio, A. *et al.* Stretching single talin rod molecules activates vinculin binding. *Science*. **323,** 638–641 (2009).
44. Roca-Cusachs, P. *et al.* Integrin-dependent force transmission to the extracellular matrix by α-actinin triggers adhesion maturation. *Proc. Natl. Acad. Sci. U. S. A.* **110,** E1361–70 (2013).
45. Kiema, T. *et al.* The molecular basis of filamin binding to integrins and competition with talin. *Mol. Cell* **21,** 337–47 (2006).
46. Lad, Y. *et al.* Structural basis of the migfilin-filamin interaction and competition with integrin beta tails. *J. Biol. Chem.* **283,** 35154–63 (2008).
47. Moik, D. V, Janbandhu, V. C. & Fässler, R. Loss of migfilin expression has no overt consequences on murine development and homeostasis. *J. Cell Sci.* **124,** 414–21 (2011).
48. Qu, H. *et al.* Kindlin-2 regulates podocyte adhesion and fibronectin matrix deposition through interactions with phosphoinositides and integrins. *J. Cell Sci.* **124,** 879–91 (2011).
49. Bledzka, K. *et al.* Spatial coordination of kindlin-2 with talin head domain in interaction with integrin β cytoplasmic tails. *J. Biol. Chem.* **287,** 24585–94 (2012).
50. Schuler, M. A., Denisov, I. G. & Sligar, S. G. Nanodiscs as a new tool to examine lipid-protein interactions. *Methods Mol Biol*. **974,** 415-33 (2013).
51. Ye, F. *et al.* Recreation of the terminal events in physiological integrin activation. *J. Cell Biol.* **188,** 157–73 (2010).
52. Mierke, C. T. *et al.* Mechano-coupling and regulation of contractility by the vinculin tail domain. *Biophys. J.* **94,** 661–70 (2008).
53. Saunders, R. M. *et al.* Role of vinculin in regulating focal adhesion turnover. *Eur. J. Cell Biol.* **85,** 487–500 (2006).
54. Cohen, D. M., Chen, H., Johnson, R. P., Choudhury, B. & Craig, S. W. Two distinct head-tail interfaces cooperate to suppress activation of vinculin by talin. *J. Biol. Chem.* **280,** 17109–17 (2005).
55. Izard, T. *et al.* Vinculin activation by talin through helical bundle conversion. **427,** 171–175 (2004).
56. Chen, H., Cohen, D. M., Choudhury, D. M., Kioka, N. & Craig, S. W. Spatial distribution and functional significance of activated vinculin in living cells. *J. Cell Biol.* **169,** 459–70 (2005).
57. Chen, H., Choudhury, D. M. & Craig, S. W. Coincidence of actin filaments and talin is required to activate vinculin. *J. Biol. Chem.* **281,** 40389–98 (2006).
58. Subauste, M. C. *et al.* Vinculin modulation of paxillin-FAK interactions regulates ERK to control survival and motility. *J. Cell Biol.* **165,** 371–81 (2004).
59. Webb, D. J. *et al.* FAK-Src signalling through paxillin, ERK and MLCK regulates adhesion disassembly. *Nat. Cell Biol.* **6,** 154–61 (2004).
60. Carisey, A. & Ballestrem, C. Vinculin, an adapter protein in control of cell adhesion signalling. *Eur. J. Cell Biol.* **90,** 157–63 (2011).

61. Le Duc, Q. *et al.* Vinculin potentiates E-cadherin mechanosensing and is recruited to actin-anchored sites within adherens junctions in a myosin II-dependent manner. *J. Cell Biol.* **189,** 1107–15 (2010).
62. Grashoff, C. *et al.* Measuring mechanical tension across vinculin reveals regulation of focal adhesion dynamics. *Nature* **466,** 263–6 (2010).
63. Geeves, M. a, Fedorov, R. & Manstein, D. J. Molecular mechanism of actomyosin-based motility. *Cell. Mol. Life Sci.* **62,** 1462–77 (2005).
64. Hodge, T. & Cope, M. J. A myosin family tree. *J. Cell Sci.* **113,** 3353–4 (2000).
65. Kull, F. J. & Endow, S. a. Force generation by kinesin and myosin cytoskeletal motor proteins. *J. Cell Sci.* **126,** 9–19 (2013).
66. Tsiavaliaris, G., Fujita-becker, S. & Manstein, D. J. Molecular engineering of a backwards-moving myosin motor. **427,** 8–11 (2004).
67. Vicente-Manzanares, M., Ma, X., Adelstein, R. S. & Horwitz, A. R. Non-muscle myosin II takes centre stage in cell adhesion and migration. *Nat. Rev. Mol. Cell Biol.* **10,** 778–90 (2009).
68. Laakso, J. M., Lewis, J. H., Shuman, H. & Ostap, E. M. Myosin I can act as a molecular force sensor. *Science* **321,** 133–6 (2008).
69. Guo, B. & Guilford, W. H. Mechanics of actomyosin bonds in different nucleotide states are tuned to muscle contraction. *Proc. Natl. Acad. Sci. U. S. A.* **103,** 9844–9 (2006).
70. Clark, K., Langeslag, M., Figdor, C. G. & van Leeuwen, F. N. Myosin II and mechanotransduction: a balancing act. *Trends Cell Biol.* **17,** 178–86 (2007).
71. Holmes KC, Popp D, Gebhard W, Kabsch W. Atomic model of the actin filament. *Nature* **347,** 44–49 (1990)
72. Sit, S.-T. & Manser, E. Rho GTPases and their role in organizing the actin cytoskeleton. *J. Cell Sci.* **124,** 679–83 (2011).
73. Nimnual, A. S., Taylor, L. J. & Bar-Sagi, D. Redox-dependent downregulation of Rho by Rac. *Nat. Cell Biol.* **5,** 236–41 (2003).
74. Abram, C. L. & Lowell, C. a. The ins and outs of leukocyte integrin signaling. *Annu. Rev. Immunol.* **27,** 339–62 (2009).
75. Stegner, D. & Nieswandt, B. Platelet receptor signaling in thrombus formation. *J. Mol. Med. (Berl).* **89,** 109–21 (2011).
76. Kim, C., Ye, F. & Ginsberg, M. H. Regulation of integrin activation. *Annu. Rev. Cell Dev. Biol.* **27,** 321–45 (2011).
77. Anthis, N. J. *et al.* The structure of an integrin/talin complex reveals the basis of inside-out signal transduction. *EMBO J.* **28,** 3623–32 (2009).
78. Ehrlicher, a J., Nakamura, F., Hartwig, J. H., Weitz, D. a & Stossel, T. P. Mechanical strain in actin networks regulates FilGAP and integrin binding to filamin A. *Nature* **478,** 260–3 (2011).
79. Hu, P. & Luo, B.-H. Integrin bi-directional signaling across the plasma membrane. *J. Cell. Physiol.* **228,** 306–12 (2013).
80. Schlaepfer, D. D., Mitra, S. K. & Ilic, D. Control of motile and invasive cell phenotypes by focal adhesion kinase. *Biochim. Biophys. Acta* **1692,** 77–102 (2004).
81. Wang, H. B., Dembo, M., Hanks, S. K. & Wang, Y. Focal adhesion kinase is involved in mechanosensing during fibroblast migration. *Proc. Natl. Acad. Sci. U. S. A.* **98,** 11295–300 (2001).
82. Schaller, M. D. Cellular functions of FAK kinases: insight into molecular mechanisms and novel functions. *J. Cell Sci.* **123,** 1007–13 (2010).
83. Boettiger, D. Mechanical control of integrin-mediated adhesion and signaling. *Curr. Opin. Cell Biol.* **24,** 592–9 (2012).
84. Krieger, C. C. *et al.* Cysteine shotgun-mass spectrometry (CS-MS) reveals dynamic sequence of protein structure changes within mutant and stressed cells. *Proc. Natl. Acad. Sci. U. S. A.* **108,** 8269–74 (2011).
85. Pasapera, A. M., Schneider, I. C., Rericha, E., Schlaepfer, D. D. & Waterman, C. M. Myosin II activity regulates vinculin recruitment to focal adhesions through FAK-mediated paxillin phosphorylation. *J. Cell Biol.* **188,** 877–90 (2010).
86. Schiller, H. B., Friedel, C. C., Boulegue, C. & Fässler, R. Quantitative proteomics of the integrin adhesome show a myosin II-dependent recruitment of LIM domain proteins. *EMBO Rep.* **12,** 259–66 (2011).
87. Gauthier, N. C., Fardin, M. A., Roca-Cusachs, P. & Sheetz, M. P. Temporary increase in plasma membrane tension coordinates the activation of exocytosis and contraction during cell spreading. *Proc. Natl. Acad. Sci. U. S. A.* **108,** 14467–72 (2011).
88. Hu, S. *et al.* Intracellular stress tomography reveals stress focusing and structural anisotropy in cytoskeleton of living cells. *Am. J. Physiol. Cell Physiol.* **285,** C1082–90 (2003).

89. Shimomura O, Johnson FH, Saiga Y. Extraction , purification and properties of aequorin, a bioluminescent protein from the luminous medusan, Aequorea. *J Cell Comp Physiol.* **59,** 223–239 (1962).
90. Olympus. Laser Scanning confocal microscopy. http://www.olympusconfocal.com/pdf [Consulta 01/01/2014]
91. Nikon. Microscopy education. http://www.microscopyu.com/ [Consulta 01/01/2014]
92. Zeiss. Education in microscopy and digital imaging. http://zeiss-campus.magnet.fsu.edu/ [Consulted 01/01/2014]
93. Stehbens, S., Pemble, H., Murrow, L. & Wittmann, T. Imaging intracellular protein dynamics by spinning disk confocal microscopy. *Methods Enzymol.* **504,** 293–313 (2012).
94. Patterson, G. H. Fluorescence microscopy below the diffraction limit. *Semin. Cell Dev. Biol.* **20,** 886–93 (2009).
95. Müller, T., Schumann, C. & Kraegeloh, A. STED microscopy and its applications: new insights into cellular processes on the nanoscale. *Chemphyschem* **13,** 1986–2000 (2012).
96. Gustafsson, M. G. Surpassing the lateral resolution limit by a factor of two using structured illumination microscopy. *J. Microsc.* **198,** 82–7 (2000).
97. Betzig, E. *et al.* Imaging intracellular fluorescent proteins at nanometer resolution. *Science* **313,** 1642–5 (2006).
98. Hess, S. T., Girirajan, T. P. K. & Mason, M. D. Ultra-high resolution imaging by fluorescence photoactivation localization microscopy. *Biophys. J.* **91,** 4258–72 (2006).
99. Rust, M. J., Bates, M. & Zhuang, X. imaging by stochastic optical reconstruction microscopy (STORM). **3,** 793–795 (2006).
100. Mattheyses, A. L., Simon, S. M. & Rappoport, J. Z. Imaging with total internal reflection fluorescence microscopy for the cell biologist. *J. Cell Sci.* **123,** 3621–8 (2010).
101. Herman, B. & Frohlich, V. E. C. Applications in Confocal Microscopy Fluorescence Resonance Energy Transfer (FRET) *Microscopy*. **10,** 1–17 (2006).
102. Pietraszewska-Bogiel, a & Gadella, T. W. J. FRET microscopy: from principle to routine technology in cell biology. *J. Microsc.* **241,** 111–8 (2011).
103. Thaler, C., Koushik, S. V, Blank, P. S. & Vogel, S. S. Quantitative multiphoton spectral imaging and its use for measuring resonance energy transfer. *Biophys. J.* **89,** 2736–49 (2005).
104. Van Munster, E. B., Kremers, G. J., Adjobo-Hermans, M. J. W. & Gadella, T. W. J. Fluorescence resonance energy transfer (FRET) measurement by gradual acceptor photobleaching. *J. Microsc.* **218,** 253–62 (2005).
105. Goedhart, J. *et al.* Bright cyan fluorescent protein variants identified by fluorescence lifetime screening. *Nat. Methods* **7,** 137–9 (2010).
106. Chan, F. T. S., Kaminski, C. F. & Kaminski Schierle, G. S. HomoFRET fluorescence anisotropy imaging as a tool to study molecular self-assembly in live cells. *Chemphyschem* **12,** 500–9 (2011).
107. Becker, N. *et al.* Molecular nanosprings in spider capture-silk threads. *Nat. Mater.* **2,** 278–83 (2003).
108. Wehrle-Haller, B. Analysis of integrin dynamics by fluorescence recovery after photobleaching. *Methods Mol. Biol.* **370,** 173–202 (2007).
109. Axelrod, D., Koppel, D. E., Schlessinger, J., Elson, E. & Webb, W. W. Mobility measurement by analysis of fluorescence photobleaching recovery kinetics. *Biophys. J.* **16,** 1055–69 (1976).
110. Zhao, F. *et al.* Roles for GP IIb/IIIa and αvβ3 integrins in MDA-MB-231 cell invasion and shear flow-induced cancer cell mechanotransduction. *Cancer Lett.* (2013).
111. Wang, D. *et al.* A stretching device for imaging real-time molecular dynamics of live cells adhering to elastic membranes on inverted microscopes during the entire process of the stretch. *Integr. Biol. (Camb).* **2,** 288–93 (2010).
112. Freis, E. D. & Heath, W. C. Hydrodynamics of Aortic Blood Flow. *Circ. Res.* **14,** 105–116 (1964).
113. Bond, L. M., Tumbarello, D. a, Kendrick-Jones, J. & Buss, F. Small-molecule inhibitors of myosin proteins. *Future Med. Chem.* **5,** 41–52 (2013).
114. Allingham, J. S., Smith, R. & Rayment, I. The structural basis of blebbistatin inhibition and specificity for myosin II. *Nat. Struct. Mol. Biol.* **12,** 378–9 (2005).
115. Sakamoto, T., Limouze, J., Combs, C. a, Straight, A. F. & Sellers, J. R. Blebbistatin, a myosin II inhibitor, is photoinactivated by blue light. *Biochemistry* **44,** 584–8 (2005).
116. Képiró, M. *et al.* Azidoblebbistatin, a photoreactive myosin inhibitor. *Proc. Natl. Acad. Sci.* **109** 9402-7 (2012).
117. Ishizaki, T. *et al.* Pharmacological properties of Y-27632, a specific inhibitor of rho-associated kinases. *Mol. Pharmacol.* **57,** 976–83 (2000).
118. Axon Med Chem . http://www.axonmedchem.com [Consulted 25/12/2013]

119. Totsukawa, G. *et al.* Distinct roles of ROCK (Rho-kinase) and MLCK in spatial regulation of MLC phosphorylation for assembly of stress fibers and focal adhesions in 3T3 fibroblasts. *J. Cell Biol.* **150,** 797–806 (2000).
120. Sigma-Aldrich. http://www.sigmaaldrich.com/ [Consulted 25/12/2013]
121. Cormack, B. P., Valdivia, R. H. & Falkow, S. FACS-optimized mutants of the green fluorescent protein (GFP). *Gene* **173,** 33–8 (1996).
122. Subach, F. V *et al.* Red fluorescent protein with reversibly photoswitchable absorbance for photochromic FRET. *Chem. Biol.* **17,** 745–55 (2010).
123. Padilla-Parra, S. & Tramier, M. FRET microscopy in the living cell: different approaches, strengths and weaknesses. *Bioessays* **34,** 369–76 (2012).
124. Ganguly, S., Clayton, A. H. a & Chattopadhyay, A. Fixation alters fluorescence lifetime and anisotropy of cells expressing EYFP-tagged serotonin1A receptor. *Biochem. Biophys. Res. Commun.* **405,** 234–7 (2011).
125. Domin, A., Lan, M. J. & Kaminski, C. Effects of fixation on cyan fluorescent protein and its fluorescence resonance energy transfer efficiency. **1,** 4–6 (2004).
126. Straight, A. F. Fluorescent protein applications in microscopy. *Methods Cell Biol.* **81,** 93–113 (2007).
127. Remington, S. J. Green fluorescent protein: a perspective. *Protein Sci.* **20,** 1509–19 (2011).
128. Kiernan, J. A. Formaldehyde , formalin , paraformaldehyde and glutaraldehyde : What they are and what they do. *Micro. tod.* **12,** 8–12 (2000).
129. Beaumont, K. G. & Mrksich, M. The mechanostability of isolated focal adhesions is strongly dependent on pH. *Chem. Biol.* **19,** 711–20 (2012).
130. Jeon, H., Kim, E. & Grigoropoulos, C. P. Measurement of contractile forces generated by individual fibroblasts on self-standing fiber scaffolds. *Biomed. Microdevices* **13,** 107–15 (2011).
131. Lavelin, I. *et al.* Differential effect of actomyosin relaxation on the dynamic properties of focal adhesion proteins. *PLoS One* **8,** e73549 (2013).
132. Lele, T. P., Thodeti, C. K., Pendse, J. & Ingber, D. E. Investigating complexity of protein-protein interactions in focal adhesions. *Biochem. Biophys. Res. Commun.* **369,** 929–34 (2008).
133. Himmel, M. *et al.* Control of high affinity interactions in the talin C terminus: how talin domains coordinate protein dynamics in cell adhesions. *J. Biol. Chem.* **284,** 13832–42 (2009).
134. Conway, D. E. *et al.* Fluid shear stress on endothelial cells modulates mechanical tension across VE-cadherin and PECAM-1. *Curr. Biol.* **23,** 1024–30 (2013).
135. Seong, J. *et al.* Detection of focal adhesion kinase activation at membrane microdomains by fluorescence resonance energy transfer. *Nat. Commun.* **2,** 406 (2011).
136. Schneider, C.A., Rasband, W.S., Eliceiri, K.W. NIH Image to ImageJ: 25 years of image analysis. *Nature Methods* **9,** 671-675 (2012)
137. Sprague, B. L. & McNally, J. G. FRAP analysis of binding: proper and fitting. *Trends Cell Biol.* **15,** 84–91 (2005).
138. Kapitza, H. G., McGregor, G. & Jacobson, K. a. Direct measurement of lateral transport in membranes by using time-resolved spatial photometry. *Proc. Natl. Acad. Sci. U. S. A.* **82,** 4122–6 (1985).
139. Veigel, C. & Schmidt, C. F. Moving into the cell: single-molecule studies of molecular motors in complex environments. *Nat. Rev. Mol. Cell Biol.* **12,** 163–76 (2011).
140. Harburger, D. S. & Calderwood, D. a. Integrin signalling at a glance. *J. Cell Sci.* **122,** 1472–1472 (2009).
141. Biocarta. Rho cell motiliy signalling pathway. http://www.biocarta.com/pathfiles/m_rhoPathway.asp [Consulted 05/11/2013]
142. Ballestrem, C. & Geiger, B. Application of microscope-based FRET to study molecular interactions in focal adhesions of live cells. *Methods Mol. Biol.* **294,** 321–34 (2005).
143. Misteli, T. Protein Dynamics: Implications for Nuclear Architecture and Gene Expression. *Science (80-.).* **291,** 843–847 (2001).
144. Terjung, S. Pepperkok, R. FRAP teaching module. http://www.embl.de/eamnet/frap/index.html [Consulted on 16/09/2013]